A symmetry-projected variational approach to the 1-dimensional Hubbard-model

K.W. Schmid, T. Dahm, J. Margueron and H. Müther
Institut für Theoretische Physik der Universität Tübingen,
Auf der Morgenstelle 14, D-72076 Tübingen, Germany

We apply a variational method devised for the nuclear many–body problem to the 1-dimensional Hubbard–model with nearest neighbor hopping and periodic boundary conditions. The test wave function consist for each state out of a single Hartree–Fock determinant mixing all the sites (or momenta) as well as the spin–projections of the electrons. Total spin and linear momentum are restored by projection methods before the variation. It is demonstrated that this approach reproduces the results of exact diagonalisations for half–filled $N = 12$ and $N = 14$ lattices not only for the energies and occupation numbers of the ground but also of the lowest excited states rather well. Furthermore, a system of 10 electrons in a $N = 12$ lattice is investigated and, finally, a $N = 30$ lattice is studied. In addition to energies and occupation numbers we present the spectral functions computed with the help of the symmetry–projected wave functions, too. Also here nice agreement with the exact results (where available) is reached.

PACS numbers: 71.10.Fd, 21.60.-n
Keywords: Lattice fermion models, Nuclear–structure models and methods

I. INTRODUCTION

Consider a finite number of N identical Fermions in a model space defined by some finite number M of suitably chosen orthonormal single Fermion basis states. Assume furthermore, that the effective Hamiltonian of these Fermions appropriate for this model space is known. Then, at least in principle, this many–Fermion problem is exactly solvable. One only has to distribute the N Fermions over the M orbitals according to the Pauli principle, i.e., construct all possible Slater–determinants, and then to diagonalize the known Hamiltonian in the resulting configuration space of dimension $\binom{M}{N}$.
The nuclear shell–model (see [1] for a recent review and references therein) is one realization of this scheme. In order to describe ground-state and low energy excited states of a nucleus Z_v valence protons and N_v valence neutrons are distributed over M_p and M_n single-particle basis states and a suitably chosen effective Hamiltonian is then diagonalized in the resulting configuration space. The dimension of this configuration space which is $\binom{M_p}{Z_v} \cdot \binom{M_n}{N_v}$, can, however, be reduced considerably, if use is made of the symmetries of the effective Hamiltonian. So, e.g., the effective nuclear many–body Hamiltonian is a scalar in normal space and thus does neither mix states with different total angular momentum nor with different z–projections of the latter. Furthermore, neglecting weak interactions, parity becomes a good quantum number, too. Consequently, the above Slater–determinants can always be coupled to configurations with definite parity and angular momentum quantum numbers and the Hamiltonian can then be diagonalized in the much smaller configuration spaces corresponding to such a symmetry representation. However, even if use is made of all the symmetries, in general the dimensions are far too large to be numerically tractable. Thus in most cases one has to rely on approximate methods, which truncate the complete shell–model expansion of the wave functions to a numerically feasible number of configurations. How this can be done without loosing the essential degrees of freedom being relevant for any particular state under consideration is the central question of nuclear structure physics.
The Hubbard–model, a schematic model developed to describe some basic features of solid state physics, is another example for the scheme outlined above. In this case N_e electrons are distributed over the N sites of a lattice and the corresponding model–Hamiltonian is then diagonalized within the resulting configuration space (see, e.g. [2] and references therein). Again, the dimension of this configuration space increases drastically with the number of lattice points N and again, even if all the available symmetries are used, the dimensions are in general far too large to allow for an exact solution. Thus again approximate methods are asked for and rather successful ones have been developed within the past [2]. The aim of the present study is to adopt an approximation scheme, which has successfully been applied in nuclear physics, and apply it to the Hubbard model to test its efficiency for this system.
One of the most successful truncation approaches to the nuclear many–body problem has been addressed in a recent review article [3]. It works with general Hartree–Fock–Bogoliubov configurations, breaking all the symmetries required by the effective nuclear many–body Hamiltonian, as basic building blocks. These symmetries are restored with the help of projection techniques and the underlying HFB–transformations as well as the configuration–mixing are then determined by variational calculations. In quantum chemistry such kind of approaches are called *unrestricted self-consistent field approximations with variation after projection* and it is known that electronic correlations can be accounted for this way by breaking symmetries [4].

Here we want to address the question how well the symmetry projected variational approach will perform when applied to the Hubbard model. For simplicity we shall restrict ourselves to the 1–dimensional Hubbard model and use only general Hartree–Fock instead of Hartree–Fock–Bogoliubov configurations in the symmetry projected variational approach. As a test we will determine energies and single-particle spectral functions and compare the results to exact results for cases, for which the exact diagonalization can be done. We will also demonstrate the feasibility of the symmetry projected variational approach for cases, which cannot be solved by brute force diagonalization.
We present the relevant formalism in sec. II. We start with a short sketch of the 1–dimensional Hubbard model with nearest neighbor hopping and periodic boundary conditions in sec. II A. In sec. II B we shall then derive the variational equations for the Hartree–Fock approach with spin– and linear momentum–projection before the variation for the ground as well as for the excited states of the considered system. How to calculate the corresponding (hole– a well as particle–) spectral functions is discussed in sec. II C. Sec. III contains some general properties of the Hubbard–model and presents then the results obtained within the variational approach for half–filled $N = 12$–, $N = 14$– and $N = 30$–lattices. Where possible these results are compared with those of complete diagonalisations. Furthermore, some results for a 10 electron system in a $N = 12$ lattice are presented. Finally, some conclusions and an outlook are given in sec. IV.

II. THEORY

A. The 1-dimensional Hubbard–model

In its simplest version [2] the effective Hamiltonian of the 1-dimensional Hubbard–model has the form

$$\hat{H} \equiv -t \sum_{j=1}^{N} \sum_{\sigma=-1/2}^{+1/2} \left\{ \hat{c}^{\dagger}_{j+1\sigma} \hat{c}_{j\sigma} + \hat{c}^{\dagger}_{j\sigma} \hat{c}_{j+1\sigma} \right\} + U \sum_{j=1}^{N} \hat{c}^{\dagger}_{j\uparrow} \hat{c}^{\dagger}_{j\downarrow} \hat{c}_{j\downarrow} \hat{c}_{j\uparrow} \, . \tag{1}$$

Here the operator $\hat{c}^{\dagger}_{j\sigma}$ creates from the particle vacuum $|0\rangle$ an electron with spin–projection $\sigma = \pm 1/2$ along an arbitrary chosen quantization axis on the site j ($j = 1, \ldots, N$), the corresponding annihilator $\hat{c}_{j\sigma}$ destroys such an electron. Obviously, these operators fulfill the standard anti–commutation relations for Fermion–operators

$$\left\{ \hat{c}^{\dagger}_{j\sigma}, \, \hat{c}_{j'\,\sigma'} \right\} \equiv \hat{c}^{\dagger}_{j\sigma} \, \hat{c}_{j'\,\sigma'} + \hat{c}_{j'\,\sigma'} \, \hat{c}^{\dagger}_{j\sigma} = \delta_{j,\,j'} \, \delta_{\sigma,\,\sigma'} \, . \tag{2}$$

The Hamiltonian (1) simulates a system of electrons in a periodic potential, in which each of the N potential wells is supposed to have only a single bound electron state, which can be occupied by at most two electrons with opposite spin–directions. In case that two electrons are occupying the same state, they feel the repulsive Coulomb–interaction ($U > 0$). Furthermore, each electron may tunnel to the neighboring well (if the corresponding site is not already filled by an electron with the same spin–projection). This so–called "nearest–neighbor–hopping" is described by the "hopping parameter" $t > 0$. As usual, all energies are measured in units of this parameter and N is supposed to be an even integer. One furthermore assumes periodic boundary conditions, i.e. the sites $N + 1$ and 1 are identical. Thus the system lives on a circle of length $L = N\Delta$. The spacing Δ is set to unity in the following. Let us for the moment consider a "half–filled" grid, i.e. $N_e = N$ electrons on the N sites. It is obvious, that for interaction strength $U = 0$ these electrons form a noninteracting "Fermi–gas" in a finite, 1–dimensional box, while for very large interaction strength ($U \to \infty$) an anti-ferromagnetic ground state with total spin $S = 0$ is to be expected [2].
We apply now the Fourier transformation

$$\hat{c}^{\dagger}_{\alpha\sigma} = \frac{1}{\sqrt{N}} \sum_{j=1}^{N} \exp\{-ik_{\alpha} \, j\} \, \hat{c}^{\dagger}_{j\sigma} \tag{3}$$

on the basis orbits ($\Delta = 1$). This yields a set of N single electron states in momentum space with momenta

$$k_{\alpha} \equiv \frac{2\pi}{N} \, \alpha \qquad \alpha = -N/2 + 1, \ldots, N/2 \, , \tag{4}$$

in terms of which the Hamiltonian (1) gets the form

$$\hat{H} = -2t \sum_{\alpha} \sum_{\sigma=-1/2}^{1/2} \cos\left(\frac{2\pi}{N} \, \alpha \right) \hat{c}^{\dagger}_{\alpha\sigma} \hat{c}_{\alpha\sigma} + \frac{U}{N} \sum_{\alpha,\,\beta,\,\gamma,\,\delta} \delta^{0,\,\pm N}_{\alpha+\beta-\gamma-\delta} \hat{c}^{\dagger}_{\alpha\uparrow} \hat{c}^{\dagger}_{\beta\downarrow} \hat{c}_{\delta\downarrow} \hat{c}_{\gamma\uparrow} \, , \tag{5}$$

where the generalized Kronecker–symbol is one, if $\alpha+\beta-\gamma-\delta$ is either 0 or $\pm N$ (because of the periodic boundary conditions), and zero else. The linear momentum quantum numbers α, β, γ, δ run all over $-N/2+1, \ldots N/2$. Because of the "cosine–dispersion" in the one–body term, the single particle spectrum contains one state with energy $-2t$ (for $\alpha = 0$), one state with energy $+2t$ (for $\alpha = N/2$) and $N-2$ two–fold degenerate states with energies $\cos([2\pi/N]\alpha)$ (for $\alpha = \pm 1, \ldots, \pm(N/2-1)$).
Obviously, the Hamiltonian (1) or (5) conserves the total number of electrons. Furthermore, it is easy to show, that it commutes with the square of the total spin operator $\hat{S}^2$ as well as with its 3–component $\hat{S}_z$ and is thus a scalar in spin–space. Hence its eigenstates can be classified according to the corresponding spin–quantum number S and are degenerate for all the $2S+1$ values of its z–projection $\Sigma = -S, ..., S$. For an even number of electrons only integer values for the total spin can occur. Since each of these spin–values has a $\Sigma = 0$ component, it is sufficient to diagonalize (1) or (5) in the space of the $\Sigma = 0$ configurations in order to obtain all the eigenstates. In contrast, for an odd number of electrons S is a half–integer, so that in this case all the configurations with $\Sigma = 1/2$ have to be used as basis states. The lowest eigenvalues and eigenvectors for such a matrix with large dimension can be obtained by applying efficient algorithms like e.g. the Lanczos–method [5]. For half–filling ($N_e = N$ even) the total number of $\Sigma = 0$ configurations to be treated is

$$n(N/2,\, \Sigma = 0) \;\equiv\; \binom{N}{N/2}^2 , \tag{6}$$

and thus increases drastically with the number N of available sites (for $N = 16$,e.g., eq. (6) yields already 165 636 900 configurations). Hence the applicability of this approach is rather limited. The situation becomes slightly better, if instead of all $\Sigma = 0$ Slater–determinants only those configurations with a definite total spin–value S are included. Again for half–filling, one obtains here dimensions of

$$n(N/2,\, S) \;\equiv\; \binom{N}{N/2-S}^2 - \binom{N}{N/2-S-1}^2 , \tag{7}$$

which for $N = 16$ still amount to 34 763 300 $S = 0$ and even 66 745 536 $S = 1$ configurations, respectively. In addition, such a procedure requires the coupling of the simple Slater–determinant to configurations with good total spin and thus complicates the calculation of the various matrix elements considerably.
There is, however, a further symmetry of the Hamiltonian, which can be used to reduce the dimension of the configuration spaces. As can be shown easily, the operator (5) commutes (modulo $\pm 2\pi$) with the Hamiltonian of total linear momentum

$$\hat{P} \;\equiv\; \sum_{\alpha,\,\sigma} \left\{ \frac{2\pi}{N}\alpha \right\} \hat{c}^{\dagger}_{\alpha\sigma}\hat{c}_{\alpha\sigma} \,, \tag{8}$$

and thus the eigenstates can be classified in addition by a momentum quantum number ξ, too. The corresponding total momentum is $k_\xi = (2\pi/N)\xi$. The total linear momentum quantum number can assume all values given in eq. (4) or, equivalently, all integer values (ξ) in between 0 and $(N-1)$, where use has been made of the periodic boundary conditions. In addition, it is immediately seen, that the Hamiltonian (5) remains unchanged, if the signs of all the linear momentum quantum numbers are flipped (because of the periodic boundary conditions $-N/2 \rightarrow -N/2+N = N/2$). Thus the states with $\xi = 1$ are degenerate with those with $\xi = N-1$, those with $\xi = 2$ with those with $\xi = N-2$, etc., while the states with $\xi = N/2$ (again, since $-N/2 \rightarrow -N/2+N = N/2$) occur only once.
For half–filling, the total number of configurations with a given total spin S and given linear momentum quantum number ξ cannot be given in a closed form but it can be easily calculated numerically. It turns out that

$$n(N/2,\, S\xi) \;\simeq\; n(N/2,\, S)/N \tag{9}$$

is a rather good first guess for all possible ξ–values, if N is sufficiently large. For $N = 16$ and $S = 0$, e.g., the dimensions for the various configuration spaces are 2 172 400 (for $\xi = 1$, 3, 5, 7, 9, 11, 13, 15), 2 173 008 (for $\xi = 2$, 6, 10, 14), 2 173 016 (for $\xi = 4$, 12) and 2 173 018 (for $\xi = 0$, 8), respectively.
However, even if spin and linear momentum are used as "good" quantum numbers, the dimension of the resulting configuration spaces still increases drastically with the number of sites. For $N = 18$ and $S = 0$ eq. (9) yields already $2.5 * 10^7$, and for $N = 30$ and $S = 0$ even $9.7 * 10^{13}$ configurations for each ξ have to be treated. Thus, at least for half–filling and $N \geq 18$, an exact solution is almost impossible even on modern computers. This statement remains valid even if we furthermore consider the symmetry of the Hubbard Hamiltonian under charge rotation and the corresponding conserved quantum numbers.

Therefore one has to rely on approximate methods, which truncate the complete expansion of the wave functions to a numerically feasible number of configurations. How this can be done without loosing the essential degrees of freedom relevant for the particular states under consideration is the central question not only for the Hubbard–model but for any other finite many–body problem as well.
One of the most favored methods for such a truncation is provided by Greens–function Monte–Carlo calculations, in which the relevant configurations are selected according to their statistical weight. This method has been applied rather successfully not only to the Hubbard–model [6] but also to the nuclear many–body problem [7]. It has, however, the limitation that only expectation values within the ground state or in some statistical assembly can be obtained. For Fermion–systems the method suffers in addition from the well–known "sign–problem". In nuclear physics both these shortcomings could be overcome in recent years by the so–called "Quantum–Monte–Carlo–Diagonalization" (QMCD) method [8], in which again the relevant configurations are selected by stochastic methods, however, the sign–problem can be bypassed and ground as well as excited states can be treated on equal footing.
However, stochastic selection is not the only promising method for truncation in finite many–body problems. Another possibility is provided by variational methods. Here one uses the most general Slater–determinants (or even generalized Slater–determinants), which can be constructed within the considered single particle space, as basic building blocks. Unfortunately, in general these configurations do break all the symmetries required by the chosen many–body Hamiltonian and hence cannot be considered as physical states but only as an approximation introduced to account for as much as possible of the correlations in as few as possible configurations. The required symmetries, however, can be restored with the help of projection techniques, and the resulting symmetry–projected configurations can then be used as test wave functions in chains of variational calculations in order to determine the underlying single particle transformations as well as the configurations mixing. Such symmetry–projected variational calculations on the basis of general Hartree–Fock–Bogoliubov configurations have been applied very successfully to the nuclear many–body problem within the last two decades (see [3] for a recent review and references therein), and it could be proven that they work equally well as alternative approaches like, e.g., the QMCD method.
In the present work we want to demonstrate that these symmetry–projected variational methods are not only useful for the nuclear many–body problem but can also be applied to other finite many–Fermion problems like the 1–dimensional Hubbard–model described above.

B. Symmetry projected Hartree–Fock

For this purpose we start by introducing "quasi–particles" of the type

$$\hat{b}^\dagger_a \equiv \sum_{\alpha=-N/2+1}^{N/2} \sum_{\sigma=-1/2}^{+1/2} D^*_{\alpha\sigma,\,a}\, \hat{c}^\dagger_{\alpha\sigma}\,, \tag{10}$$

where D is a linear $(2N \times 2N)$ transformation, which has to be unitary

$$D^\dagger D \;=\; D D^\dagger \;=\; \mathbf{1}_{2N}\,, \tag{11}$$

in order to conserve the Fermion anticommutation relations for the quasi–particle creators (10) and the corresponding annihilators. Eqs. (10) and (11) describe a general Hartree–Fock (HF) type transformation. It should be stressed here, that eq. (10) could still be generalized by including linear combinations of the annihilators on the right hand side. This would result in a so–called Hartree–Fock–Bogoliubov (HFB) transformation as used, e.g., in the approaches reviewed in ref. [3]. In the present paper, however, we shall restrict ourselves to the simpler HF–transformations only. Note, that nevertheless the transformation (10) mixes all the linear momentum quantum numbers as well as the spin–projections of the basis states (3).
In the usual Hartree–Fock approach one searches then for the optimal one–determinant representation of the N_e–electron ground state

$$|D\rangle \;=\; \left\{ \prod_{h=1}^{N_e} \hat{b}^\dagger_h \right\} |0\rangle\,, \tag{12}$$

in which the energetically lowest N_e states $\hat{b}^\dagger_h$ $(h = 1, \ldots, N_e)$ of the form (10) are occupied and the remaining $2N - N_e$ states $\hat{b}^\dagger_p$ $(p = N_e + 1, \ldots, 2N)$ are empty. In the following the notation h, h', ... is always used for the occupied states, while the unoccupied ones will be denoted by p, p', ..., respectively.
Obviously, the determinant (12) conserves the total number of electrons (N_e) but is neither an eigenstate of the square of the total spin operator $\hat{S}^{\,2}$ nor of its 3–component $\hat{S}_z$ nor of the total linear momentum operator (8). These

symmetries have therefore to be restored with the help of projection techniques. For the spin–quantum numbers this can be achieved via Villars' [9] famous projection operator

$$\hat{P}^S_{\Sigma,\Sigma'} \equiv \frac{2S+1}{8\pi^2} \int d\Omega \, D^{S^*}_{\Sigma,\Sigma'}(\Omega) \, \hat{R}_S(\Omega) \,, \tag{13}$$

where $\hat{R}_S(\Omega)$ is the rotation operator in spin–space, the Wigner–function $D^S_{\Sigma,\Sigma'}(\Omega)$ its representation in spin–eigenstates and the integral has to be taken over the full range of the three Euler–angles. Because of the non–abelian nature of the rotation group, (13) is not a true projector in the strict mathematical sense. In order to achieve independence of the choice of direction for the "intrinsic" quantization axis one is forced to use the linear combination

$$|D;\, N_e S \Sigma\rangle \;=\; \sum_{\Sigma'=-S}^{+S} \hat{P}^S_{\Sigma,\Sigma'} |D\rangle \, f_{\Sigma'} \tag{14}$$

as test wave function in the variation with the mixing coefficients f to be treated as additional variational variables. In a similar way the total linear momentum can be restored. This is done via the operator

$$\hat{C}(\xi) \;\equiv\; \frac{1}{N} \sum_{j=1}^{N} \exp\left\{ i \left(\hat{P} - \frac{2\pi}{N} \xi \right) j \right\} , \tag{15}$$

which projects the determinant (12) on the component with linear momentum $k = (2\pi/N)\xi$. The operator (15) is the finite, 1–dimensional limit of the general operator restoring Galilean invariance discussed, e.g., in ref. [3]. In contrast to nuclear systems where the Galilean principle of relativity imposes $k = 0$, lattice systems allow solutions with $k > 0$: the Hamiltonian (1) or (5) has to be considered on the (infinitely heavy) background of the ions providing the periodic potential. This background can absorb any change of linear momentum of the electrons easily so that Galilean invariance for the total system is always ensured. It should be stressed furthermore, that the spin–projection and the linear momentum projection have to be performed *before* the variation. Then the correct moment of inertia and mass is restored [10].
Using (15) in addition to (14) we obtain the projected determinant

$$|D;\, N_e \xi S \Sigma\rangle \;=\; \sum_{\Sigma'=-S}^{+S} \hat{P}^S_{\Sigma,\Sigma'} \hat{C}(\xi) |D\rangle \, f_{\Sigma'} \tag{16}$$

as ansatz for our test wave function. The corresponding energy functional

$$E \;\equiv\; \frac{\langle D;\, N_e \xi S(\Sigma) | \hat{H} | D;\, N_e \xi S(\Sigma) \rangle}{\langle D;\, N_e \xi S(\Sigma) | D;\, N_e \xi S(\Sigma) \rangle} \,, \tag{17}$$

where the spin–projection Σ has been put in parentheses since the total energy does not depend on this quantum number, has now to be minimized with respect to the mixing coefficients f as well as to the underlying HF–transformation D.
Variation with respect to the f's yields the generalized eigenvalue problem

$$(H \,-\, EN) f \;=\; 0 \,, \tag{18}$$

with the constraint

$$f^\dagger N f \;=\; \mathbf{1}_{2S+1} \tag{19}$$

ensuring the orthonormality of the solutions, and the $(2S+1)\times(2S+1)$–dimensional square matrices N and H given by

$$N_{\Sigma,\,\Sigma'} \;\equiv\; \langle D | \hat{P}^S_{\Sigma,\Sigma'} \hat{C}(\xi) | D \rangle \tag{20}$$

and

$$H_{\Sigma,\,\Sigma'} \;\equiv\; \langle D | \hat{H} \hat{P}^S_{\Sigma,\Sigma'} \hat{C}(\xi) | D \rangle \,, \tag{21}$$

respectively. The matrices N and H are hermitian and the overlap matrix (20) is furthermore positive definite. In eqs. (20) and (21) the obvious quantum numbers S and ξ have been suppressed. In the following only the energetically lowest solution of eq. (18) is kept.

The minimization of the energy functional (17) with respect to arbitrary variations of the underlying HF– transformation D is more involved. This transformation has to be unitary and thus not all of the $2N \times 2N$ matrix elements of D are linearly independent. Nevertheless, an unconstrained minimization of the functional (17) can still be performed, if one parameterizes the underlying HF–transformation via Thouless' theorem [11], which states that any HF–determinant $|D_d\rangle$ can be represented in terms of the creation and annihilation operators of some reference determinant $|D_0\rangle$ via

$$|D_d\rangle \;=\; c(d) \exp\left\{ \sum_{p,h} \; d_{ph} \hat{b}_p^\dagger(D_0) \hat{b}_h(D_0) \right\} |D_0\rangle \,, \tag{22}$$

provided that the two determinants are non–orthogonal, since

$$c(d) \;=\; \langle D_0 | D_d \rangle \,. \tag{23}$$

The creation operators belonging to the HF–determinant $|D_d\rangle$ are then related to those of the reference determinant $|D_0\rangle$ via

$$\hat{b}_h^\dagger(D_d) \;=\; \sum_{h'} [L^{-1}]_{hh'} \left(\hat{b}_{h'}^\dagger(D_0) \;+\; \sum_{p'} \; d_{p'h'} \hat{b}_{p'}^\dagger(D_0) \right) \tag{24}$$

for the occupied and

$$\hat{b}_p^\dagger(D_d) \;=\; \sum_{p'} [M^{-1}]_{pp'} \left(\hat{b}_{p'}^\dagger(D_0) \;-\; \sum_{h'} \; d^*_{p'h'} \hat{b}_{h'}^\dagger(D_0) \right) \tag{25}$$

for the unoccupied states, respectively. They are now given in terms of the $(2N - N_e) \cdot N_e$ linear independent variables d_{ph}. The lower triangular $(N_e \times N_e)$ matrix L in (24) is defined by the expression

$$\mathbf{1}_{N_e} \;+\; d^T d^* \;=\; L L^\dagger \,, \tag{26}$$

while the lower triangular $((2N - N_e) \times (2N - N_e))$ matrix M out of (25) can be obtained from the solution of the equation

$$\mathbf{1}_{2N-N_e} \;+\; d^* d^T \;=\; M M^\dagger \,. \tag{27}$$

Both, eqs. (26) and (27), are usual Cholesky decompositions.
The variational equations resulting from the minimization of the energy functional (17) with respect to the HF–transformation now assume the form

$$\frac{\partial E}{\partial d_{ph}} \;=\; \left[M^{-1^\dagger} \, G \, L^{-1} \right]_{ph} \;\equiv\; 0 \,, \tag{28}$$

where the $((2N - N_e) \times N_e)$ matrix G is defined by

$$G_{ph} \;\equiv\; \sum_{\Sigma,\, \Sigma'} \; f^*_\Sigma \, \langle D | (\hat{H} \;-\; E\mathbf{1}) \hat{P}^S_{\Sigma,\Sigma'} \hat{C}(\xi) \, \hat{b}_p^\dagger(D) \, \hat{b}_h(D) | D \rangle \, f_{\Sigma'} \,. \tag{29}$$

Once one has reached the solution not only the "global" gradient vector (28) but also the "local" one (29) does vanish identically. This vanishing of the gradient vector (29) is a sort of "generalized Brillouin theorem" [11] : it describes the stability of the symmetry–projected HF–solution with respect to arbitrary symmetry–projected one particle–one hole excitations.
For any given S and ξ, the simultaneous solution of the set of eqs. (18), (19) and (28) yields the optimal representation of the energetically lowest state by one single symmetry–projected HF–type configuration. This corresponds to the so–called VAMPIR (**V**ariation **A**fter **M**ean–field **P**rojection **I**n **R**ealistic model spaces) approach out of ref. [3], though restricted here to a HF–type instead of HFB–type transformations. Since D (and hence d) as well as f are essentially complex matrices this solution results from the minimization of a function of $m = 2 \cdot (2N - N_e) \cdot N_e \cdot$ real variables, if even N_e and $S = 0$ is considered, while in general for $S > 0$ and arbitrary N_e, $(4S + 1) + m$ real variables have to be treated. For this minimization a quasi–Newton procedure (see, e.g., [12, 13]) is used.

Excited states with the same quantum numbers S and ξ can be treated in a similar fashion, if one ensures the orthogonality with respect to the solutions already obtained. For the first excited state ($n = 2$) this can be achieved with the help of the projection operator

$$\hat{T}_{n-1} \equiv \sum_{i=1}^{n-1} |D^i;\, N_e \xi S \Sigma\rangle \langle D^i;\, N_e \xi S \Sigma| \,, \tag{30}$$

which projects on the lowest solution (D^1, f^1) of the form (16). For the variational calculation then instead of (16) we use its complement

$$|D^n;\, N_e \xi S \Sigma\rangle \equiv (1 - \hat{T}) \sum_{\Sigma'=-S}^{+S} \hat{P}^S_{\Sigma,\Sigma'} \hat{C}(\xi) |D^n\rangle \, f^n_{\Sigma'} \tag{31}$$

as a test wave function for the variational calculation. The procedure (30), (31) can be repeated for the second excited state ($n = 3$), etc., up to the n lowest (orthonormal) states. Finally, the residual interaction between these n states is diagonalized. This corresponds closely to the EXCITED VAMPIR approach from ref. [3].
Furthermore, we would like to stress, that if a description by one single symmetry–projected determinant for each state is not sufficient, further correlations can easily be accounted for by successive variational calculations for additional determinants as done in the FED (from **FE**w **D**eterminants) EXCITED VAMPIR approach out of ref. [3]. This, however, has not been done in the present work since one determinant gives already a good accuracy, as we will see below.
Left to be computed are now the symmetry projected matrices (20) and (21) generalized to two different determinants $|D^i\rangle$ and $|D^k\rangle$ on both sides, because of the eventual use of (31) instead of (16) as test wave function and of more than one determinant for the description of the $N_e \pm 1$–electron systems as discussed in sec. II C. Furthermore, the corresponding gradient vectors occurring in eq. (29) have to be calculated. One obtains successively

$$\langle D^i | \hat{P}^S_{\Sigma,\Sigma'} \hat{C}(\xi) | D^k \rangle = \frac{1}{N} \sum_{j=1}^{N} \exp\left\{ -i \frac{2\pi}{N} \xi j \right\} \frac{2S+1}{8\pi^2} \int d\Omega \, D^{S\,*}_{\Sigma,\Sigma'}(\Omega) \, n^{ik}(\Omega,\, j) \,, \tag{32}$$

$$\begin{aligned} \langle D^i | \hat{H} \hat{P}^S_{\Sigma,\Sigma'} \hat{C}(\xi) | D^k \rangle &= \frac{1}{N} \sum_{j=1}^{N} \exp\left\{ -i \frac{2\pi}{N} \xi j \right\} \frac{2S+1}{8\pi^2} \int d\Omega \, D^{S\,*}_{\Sigma,\Sigma'}(\Omega) \cdot \\ &\quad \cdot h^{ik}(\Omega,\, j) n^{ik}(\Omega,\, j) \,, \end{aligned} \tag{33}$$

and,

$$\begin{aligned} \langle D^i | \hat{P}^S_{\Sigma,\Sigma'} \hat{C}(\xi)\, \hat{b}^\dagger_p(D^k)\, \hat{b}_h(D^k) | D^k \rangle &= \frac{1}{N} \sum_{j=1}^{N} \exp\left\{ -i \frac{2\pi}{N} \xi j \right\} \frac{2S+1}{8\pi^2} \int d\Omega \, D^{S\,*}_{\Sigma,\Sigma'}(\Omega) \cdot \\ &\quad \cdot n^{ik}_{ph}(\Omega,\, j) n^{ik}(\Omega,\, j) \,, \end{aligned} \tag{34}$$

$$\begin{aligned} \langle D^i | \hat{H} \hat{P}^S_{\Sigma,\Sigma'} \hat{C}(\xi)\, \hat{b}^\dagger_p(D^k)\, \hat{b}_h(D^k) | D^k \rangle &= \frac{1}{N} \sum_{j=1}^{N} \exp\left\{ -i \frac{2\pi}{N} \xi j \right\} \frac{2S+1}{8\pi^2} \int d\Omega \, D^{S\,*}_{\Sigma,\Sigma'}(\Omega) \cdot \\ &\quad \cdot h^{ik}_{ph}(\Omega,\, j) n^{ik}(\Omega,\, j) \,. \end{aligned} \tag{35}$$

In these expressions the spin–rotated and shifted overlap–functions are given by

$$n^{ik}(\Omega,\, j) \equiv \det{}_{N_e} X^{ik}(\Omega,\, j) \,, \tag{36}$$

and

$$n^{ik}_{ph}(\Omega,\, j) \equiv \sum_{h' \in |D^i\rangle} [X^{ik}_{h,h'}(\Omega,\, j)]^{-1} \, X^{ik}_{h',p}(\Omega,\, j) \,, \tag{37}$$

respectively. The determinant in eq. (36) has to be taken for the occupied $N_e \times N_e$–dimensional part of the $(2N \times 2N)$–matrix X^{ik}

$$X^{ik}_{ab} \equiv \sum_{\alpha,\, \sigma\sigma'} D^i_{\alpha\sigma,\, a} \, S_{\alpha\sigma,\, \alpha\sigma'}(\Omega,\, j) \, D^{k\,*}_{\alpha\sigma',\, b} \tag{38}$$

and in eq. (37) the indices h and p run over all the occupied and unoccupied states of the HF–determinant $|D^k\rangle$, respectively. $(X^{ik})^{-1}$ denotes the inverse of the occupied part of the matrix (38) and

$$S_{\alpha\sigma,\,\alpha\sigma'}(\Omega,\,j)\;\equiv\;D^{1/2}_{\sigma,\,\sigma'}(\Omega)\,\exp\left\{i\frac{2\pi}{N}\alpha\,j\right\}\,. \tag{39}$$

In eq. (33) the spin–rotated and shifted matrix elements of the Hamiltonian involve also

$$h^{ik}(\Omega,\,j)\;\equiv\;\frac{1}{2}\left\{t^{ik}(\Omega,\,j)\;+\;\sum_{\alpha\sigma,\,\gamma\sigma'}\tilde{\Gamma}^{ik}_{\alpha\sigma,\,\gamma\sigma'}(\Omega,\,j)\tilde{\rho}^{ki}_{\gamma\sigma',\,\alpha\sigma}(\Omega,\,j)\right\}\,, \tag{40}$$

where

$$t^{ik}(\Omega,\,j)\;\equiv\;\sum_{\alpha\sigma}\left[-2t\cos\left(\frac{2\pi}{N}\alpha\right)\right]\tilde{\rho}^{ki}_{\alpha\sigma,\,\alpha\sigma}(\Omega,\,j)\,, \tag{41}$$

$$\begin{aligned}\tilde{\Gamma}^{ik}_{\alpha\sigma,\,\gamma\sigma'}(\Omega,\,j)\;\equiv\;&\delta_{\sigma,\,\sigma'}\left\{\delta_{\alpha,\,\gamma}\left[-2t\cos\left(\frac{2\pi}{N}\alpha\right)\right]\;+\;\sum_{\beta\delta}\frac{U}{N}\delta^{0;\pm N}_{\alpha+\beta-\gamma-\delta}\tilde{\rho}^{ki}_{\delta-\sigma,\,\beta-\sigma}(\Omega,\,j)\right\}\\&-(1-\delta_{\sigma,\,\sigma'})\left\{\sum_{\beta\delta}\frac{U}{N}\delta^{0;\pm N}_{\alpha+\beta-\gamma-\delta}\tilde{\rho}^{ki}_{\delta\sigma,\,\beta\sigma}(\Omega,\,j)\right\},\end{aligned} \tag{42}$$

and

$$\tilde{\rho}^{ki}_{\gamma\sigma',\,\alpha\sigma}(\Omega,\,j)\;\equiv\;\sum_{\sigma''}S_{\gamma\sigma',\,\gamma\sigma''}(\Omega,\,j)\sum_{hh'}D^{k^*}_{\gamma\sigma'',\,h}[X^{ik}_{h,\,h'}(\Omega,\,j)]^{-1}D^{i}_{\alpha\sigma,\,h'}\,. \tag{43}$$

Furthermore, introducing the definitions

$$y^{ki}_{h,\,\alpha\sigma}(\Omega,\,j)\;\equiv\;\sum_{h'}[X^{ik})^{-1}_{h,\,h'}(\Omega,\,j)]^{-1}D^{i}_{\alpha\sigma,\,h'} \tag{44}$$

for all the occupied states h in the Slater–determinant $|D^k\rangle$, and

$$\tilde{\omega}^{ki}_{\gamma\sigma',\,p'}(\Omega,\,j)\;\equiv\;\sum_{\delta\sigma''}[\mathbf{1}\;-\;\tilde{\rho}^{ki}(\Omega,\,j)]_{\gamma\sigma',\,\delta\sigma''}\sum_{\sigma'''}S_{\delta\sigma'',\,\delta\sigma'''}(\Omega,\,j)D^{k^*}_{\delta\sigma''',\,p'} \tag{45}$$

for all the unoccupied states p' belonging again to the transformation D^k, one can write the spin–rotated and shifted energy function out of eq. (35) as

$$h^{ik}_{ph}(\Omega,\,j)\;\equiv\;n^{ik}_{ph}(\Omega,\,j)h^{ik}(\Omega,\,j)\;+\;\sum_{\alpha\sigma,\,\gamma\sigma'}y^{ki}_{h,\,\alpha\sigma}(\Omega,\,j)\tilde{\Gamma}^{ik}_{\alpha\sigma,\,\gamma\sigma'}(\Omega,\,j)\tilde{\omega}^{ki}_{\gamma\sigma',\,p}(\Omega,\,j)\,. \tag{46}$$

The above described variational procedure will be denoted by LMSPHF (from **L**inear **M**omentum and **S**pin **P**rojected **H**artree–**F**ock) in the following.
Finally, it should be stressed that this procedure can be used for any number of electrons $N_e = 1,\ldots,2N$. As we already mentioned, for odd N_e the spin quantum numbers S and Σ are half–integer numbers.

C. Spectral functions

Let us now assume that we have obtained the ground state for an even number of electrons N_e on a lattice with N sites solving the variational equations out of the sec. II B. As we shall see in sec. III, this ground state has always total spin $S = 0$ but not necessarily linear momentum quantum number $\xi_0 = 0$. For instance, in the case of half–filling and $N/2$ even the ground state is obtained for $\xi_0 = N/2$. The underlying HF–transformation will be denoted by D^1 and the total energy by E_0. For $S = 0$, there exists only a single coefficient f_0, which is uniquely determined by the normalization

$$f_0\;\equiv\;n_0^{-1/2}\;=\;\langle D^1|\hat{P}^0_{0,0}\hat{C}(\xi_0)|D^1\rangle^{-1/2}\,. \tag{47}$$

The projected ground state of the N_e–electron system can thus be written as

$$|D^1;\, N_e \xi_0 S = \Sigma = 0\rangle \;=\; \hat{P}^0_{0,\,0}\, \hat{C}(\xi_0)\, |D^1\rangle\, n_0^{-1/2}\,. \tag{48}$$

We shall now approximate the $(N_e - 1)$–electron system (characterized by $S = 1/2$ and ξ_{-1}) by

$$|\tilde{h}\,;\, N_e - 1\, \xi_{-1}\, S = 1/2\, \sigma\rangle \;\equiv\; \sum_{i=1}^{m} \sum_{h=1}^{N_e} \sum_{\sigma'=-1/2}^{1/2} \hat{P}^{1/2}_{\sigma,\,\sigma'} \hat{C}(\xi_{-1}) \hat{b}_h(D^i) |D^i\rangle\, f_{ih\sigma',\,\tilde{h}}\,, \tag{49}$$

where $|D^1\rangle$ refers to the HF–determinant for the N_e–electron ground state solution, while $|D^i\rangle$ for $i = 2, \ldots, m$ refer to the determinants obtained for the lowest $m-1$ excited states (which may correspond to different spin– and linear momentum quantum numbers than the ground state one's). The mixing coefficients f are then obtained by solving a generalized eigenvalue problem similar to eq. (18)

$$(H \;-\; E_{\tilde{h}} N) f \;=\; 0 \tag{50}$$

with the constraint

$$f^\dagger N f \;=\; \mathbf{1}_{2m \cdot N_e}\,. \tag{51}$$

The overlap– and Hamiltonian–matrices are given by

$$\begin{aligned} N_{ih\sigma,\,kh'\sigma'} \;\equiv\; \frac{1}{N} \sum_{j=1}^{N} \exp\left\{-i \tfrac{2\pi}{N} \xi_{-1}\, j\right\} \tfrac{2}{8\pi^2} \int d\Omega D^{1/2^*}_{\sigma,\,\sigma'}(\Omega) \cdot \\ \cdot\, n^{ik}(\Omega,\, j) n^{ik}_{h,\,h'}(\Omega,\, j) \end{aligned} \tag{52}$$

and

$$\begin{aligned} H_{ih\sigma,\,kh'\sigma'} \;\equiv\; \frac{1}{N} \sum_{j=1}^{N} \exp\left\{-i \tfrac{2\pi}{N} \xi_{-1}\, j\right\} \tfrac{2}{8\pi^2} \int d\Omega D^{1/2^*}_{\sigma,\,\sigma'}(\Omega) \cdot \\ \cdot\, n^{ik}(\Omega,\, j) h^{ik}_{h,\,h'}(\Omega,\, j)\,, \end{aligned} \tag{53}$$

where the short–hand notations in the integrands are defined by

$$n^{ik}_{h,\,h'}(\Omega,\, j) \;\equiv\; [X^{ik}_{h',\,h}(\Omega,\, j)]^{-1} \tag{54}$$

and

$$h^{ik}_{h,\,h'}(\Omega,\, j) \;\equiv\; [X^{ik}_{h',\,h}(\Omega,\, j)]^{-1} h^{ik}(\Omega,\, j) \;-\; \sum_{\alpha\sigma,\,\gamma\sigma'} y^{ki}_{h',\,\alpha\sigma}(\Omega,\, j) \tilde{\Gamma}^{ik}_{\alpha\sigma,\,\gamma\sigma'}(\Omega,\, j) z^{ki}_{\gamma\sigma',\,h}(\Omega,\, j)\,, \tag{55}$$

respectively. Here

$$z^{ki}_{\gamma\sigma',\,h}(\Omega,\, j) \;\equiv\; \sum_{h'',\,\sigma''} S_{\gamma\sigma',\,\gamma\sigma''}(\Omega,\, j) D^{k^*}_{\gamma\sigma'',\,h''} [X^{ik}_{h'',\,h}(\Omega,\, j)]^{-1}\,, \tag{56}$$

and all the other functions are defined in sec. II B. For each possible linear momentum quantum number ξ_{-1} the eqs. (50) and (51) yield $2m \cdot N_e$ solutions $\tilde{h}$ with $S = 1/2$ and energies $E_{\tilde{h}}$.
Similarly, the $N_e + 1$–electron system (characterized by $S = 1/2$ and ξ_{+1}) will be approximated by

$$|\tilde{p}\,;\, N_e + 1\, \xi_{+1}\, S = 1/2\, \sigma\rangle \;\equiv\; \sum_{i=1}^{m} \sum_{p=N_e+1}^{2N} \sum_{\sigma'=-1/2}^{1/2} \hat{P}^{1/2}_{\sigma,\,\sigma'} \hat{C}(\xi_{+1}) \hat{b}^\dagger_p(D^i) |D^i\rangle\, g_{ip\sigma',\,\tilde{p}}\,, \tag{57}$$

where again $|D^1\rangle$ refers to the HF–determinant for the N_e–electron ground state solution, while the $|D^i\rangle$ for $i = 2, \ldots, m$ are taken from the lowest $m-1$ excited states. The mixing coefficients g are obtained by solving a generalized eigenvalue problem

$$(H \;-\; E_{\tilde{p}} N) g \;=\; 0 \tag{58}$$

with the constraint

$$g^{\dagger} N g \;=\; \mathbf{1}_{2m\cdot(2N-N_e)}\,. \tag{59}$$

The overlap– and Hamiltonian matrices are given by

$$\begin{aligned} N_{ip\sigma,\,kp'\sigma'} \;\equiv\; \frac{1}{N}\;\sum_{j=1}^{N}\exp\left\{-i\tfrac{2\pi}{N}\xi_{+1}\,j\right\}\tfrac{2}{8\pi^2}\int d\Omega D^{1/2^*}_{\sigma,\,\sigma'}(\Omega)\cdot \\ \cdot\, n^{ik}(\Omega,\,j) n^{ik}_{p,\,p'}(\Omega,\,j) \end{aligned} \tag{60}$$

and

$$\begin{aligned} H_{ip\sigma,\,kp'\sigma'} \;\equiv\; \frac{1}{N}\;\sum_{j=1}^{N}\exp\left\{-i\tfrac{2\pi}{N}\xi_{+1}\,j\right\}\tfrac{2}{8\pi^2}\int d\Omega D^{1/2^*}_{\sigma,\,\sigma'}(\Omega)\cdot \\ \cdot\, n^{ik}(\Omega,\,j) h^{ik}_{p,\,p'}(\Omega,\,j)\,, \end{aligned} \tag{61}$$

where the short–hand notations in the integrands are defined by

$$n^{ik}_{p,\,p'}(\Omega,\,j) \;\equiv\; X^{ik}_{p,\,p'}(\Omega,\,j) \;-\; \sum_{h,\,h'} X^{ik}_{p,\,h}[X^{ik}_{h,\,h'}(\Omega,\,j)]^{-1} X^{ik}_{h',\,p'}(\Omega,\,j) \tag{62}$$

and

$$h^{ik}_{p,\,p'}(\Omega,\,j) \;\equiv\; n^{ik}_{p,\,p'}(\Omega,\,j) h^{ik}(\Omega,\,j) \;+\; \sum_{\alpha\sigma,\,\gamma\sigma'} \omega^{ik}_{p,\,\alpha\sigma}(\Omega,\,j)\tilde{\Gamma}^{ik}_{\alpha\sigma,\,\gamma\sigma'}(\Omega,\,j)\tilde{\omega}^{ki}_{\gamma\sigma',\,p'}(\Omega,\,j)\,, \tag{63}$$

respectively. Furthermore,

$$\omega^{ik}_{p,\,\alpha\sigma}(\Omega,\,j) \;\equiv\; \sum_{\beta,\,\sigma'} D^{i}_{\beta\sigma',\,p}[\mathbf{1} \;-\; \tilde{\rho}^{ki}(\Omega,\,j)]_{\beta\sigma',\,\alpha\sigma}\,, \tag{64}$$

and all the other functions are again defined in sec. II B. For each possible linear momentum quantum number ξ_{+1} the eqs. (58) and (59) yield $2m\cdot(2N-N_e)$ solutions $\tilde{p}$ with $S=1/2$ and energies $E_{\tilde{p}}$.
Now the hole–spectral functions can be calculated. The spectral function for hole states, $S_{\tilde{h}}(k,\,\epsilon_{\tilde{h}})$, is defined by

$$\begin{aligned} \sqrt{S_{\tilde{h}}(k,\,\epsilon_{\tilde{h}})} \;&\equiv\; \langle \tilde{h}\,;\, N_e-1\,\xi_{-1}\,S=1/2||\,\hat{c}_{\xi_0-\xi_{-1}}\,||D^1;\,N_e\,\xi_0\,S=0\rangle \\ &=\; -\sqrt{2}n_0^{-1/2}\sum_{i=1}^{m}\sum_{h=1}^{N_e}\sum_{\sigma=-1/2}^{1/2} f^{1/2\,\xi_{-1}{}^*}_{ih\sigma,\,\tilde{h}}\cdot \\ &\quad\cdot\frac{1}{N}\sum_{j=1}^{N}\exp\left\{-i\frac{2\pi}{N}\xi_{-1}\,j\right\}\frac{1}{8\pi^2}\sum_{\sigma'=-1/2}^{1/2}\int d\Omega D^{1/2^*}_{\sigma,\,\sigma'}(\Omega)\cdot \\ &\quad\cdot\left[\sum_{h'=1}^{N_e}(-1)^{1/2-\sigma'}D^{1^*}_{\xi_0-\xi_{-1}\,-\sigma',\,h'}(X^{i1})^{-1}_{h',\,h}(\Omega,\,j)\right] n^{i1}(\Omega,\,j)\,, \end{aligned} \tag{65}$$

where $k=(2\pi/N)\xi_{-1}$ and $\epsilon_{\tilde{h}}=E_0-E_{\tilde{h}}$. Similarly, the particle spectral function can be obtained from

$$\begin{aligned} \sqrt{S_{\tilde{p}}(k,\,\epsilon_{\tilde{p}})} \;&\equiv\; \langle \tilde{p}\,;\, N_e+1\,\xi_{+1}\,S=1/2||\,\hat{c}^{\dagger}_{\xi_{+1}-\xi_0}\,||D^1;\,N_e\,\xi_0\,S=0\rangle \\ &=\; -\sqrt{2}n_0^{-1/2}\sum_{i=1}^{m}\sum_{p=N_e+1}^{2N}\sum_{\sigma=-1/2}^{1/2} g^{1/2\,\xi_{+1}{}^*}_{ip\sigma,\,\tilde{p}}\cdot \\ &\quad\cdot\frac{1}{N}\sum_{j=1}^{N}\exp\left\{-i\frac{2\pi}{N}\xi_{+1}\,j\right\}\frac{1}{8\pi^2}\sum_{\sigma'=-1/2}^{1/2}\int d\Omega D^{1/2^*}_{\sigma,\,\sigma'}(\Omega)\cdot \\ &\quad\cdot\left[\sum_{p'=N_e+1}^{2N} n^{i1}_{p,\,p'}(\Omega,\,j)D^{1}_{\xi_{+1}-\xi_0\,\sigma',\,p'}\right] n^{i1}(\Omega,\,j)\,, \end{aligned} \tag{66}$$

where now $k = (2\pi/N)\xi_{+1}$ and $\epsilon_{\tilde{p}} = E_{\tilde{p}} - E_0$.
The sum

$$\sum_{\tilde{h}=1}^{2m\cdot N_e} S_{\tilde{h}}(k,\, \epsilon_{\tilde{h}}) \equiv n(k = (2\pi/N)\xi_{-1}) \tag{67}$$

gives the occupation number of the basis state (3) in the ground state of the N_e–electron system. Here instead of using $\xi_{-1} = 0, \ldots, N-1$, we use the equivalent representation $\xi_{-1} = -N/2+1, \ldots, N/2$.
Furthermore, for plotting the spectral functions versus the linear momentum k and excitation energy $\omega = \epsilon_{\tilde{h}}$ (or $= \epsilon_{\tilde{p}}$) it is useful to introduce some artificial width for each state in order to obtain continuous functions of the excitation energy. For this purpose we use a Lorentzian shape with fixed width of 0.05 t for each hole (or particle) state. This also simplifies the representation of the density of states

$$N(\omega) \equiv \sum_{\alpha=-N/2+1}^{N/2} \left[S_{(\tilde{h})}((2\pi/N)\alpha,\, \omega) + S_{(\tilde{p})}((2\pi/N)\alpha,\, \omega) \right] . \tag{68}$$

where the indices $\tilde{h}$ and $\tilde{p}$ have been put here in parentheses, since they are absorbed now in the continuous variable ω.

In order to determine the hole spectral functions from an exact (Lanczos) solution, we start with the exact ground-state of the system with N_e electrons, $|N_e\rangle_0$, which is represented by a linear combination of the basic configurations and apply the annihilation for an electron with spin projection σ and momentum $\alpha = \xi_0 - \xi_{-1}$

$$\hat{c}_{\alpha,\sigma}|N_e\rangle_0 = \eta_\alpha |N_e - 1, \xi_{-1}, S = 1/2\rangle_1 . \tag{69}$$

The resulting state $|N_e - 1, \xi_{-1}, S = 1/2\rangle_1$ is a state with $N_e - 1$ electrons and well defined quantum numbers for the momentum (ξ_{-1}) and spin. The constant η_α has been introduced to normalize the state. This state is in general not an eigenstate of the Hamiltonian, but it can be used as a starting point to generate further states $|N_e - 1, \xi_{-1}, S = 1/2\rangle_i$ with the same quantum numbers by means of the Lanczos method[14]. A diagonalisation of the Hamiltonian in the space which is generated by these basis states $|N_e - 1, \xi_{-1}, S = 1/2\rangle_i$ for $i = 1 \ldots \nu$ will lead to ν eigenvalues ε^i_α and eigenstates $|\varepsilon^i_\alpha\rangle$, which converge with increasing ν to the exact solutions for the system with $N_e - 1$ electrons. The spectral function for the hole states can now be expressed as

$$S_h((2\pi/N)\alpha, \omega) = \eta^2_\alpha \sum_{i=1}^{\nu} \left| \langle \varepsilon^i_\alpha | N_e - 1, \xi_{-1}, S = 1/2\rangle_0 \right|^2 \delta\left(\omega - \varepsilon^i_\alpha\right) . \tag{70}$$

This means that the occupation probability $n((2\pi/N)\alpha)$ is determined by the square of the normalisation constant η_α defined in eq. (69) and the overlap of the states $|\varepsilon^i_\alpha\rangle$ with the starting vector for the Lanczos iteration $|N_e - 1, \xi_{-1}, S = 1/2\rangle_1$ defines the spectral strength at the energy $\omega = \varepsilon^i_\alpha$. The result for the spectral function converges very rapidly with the number of iterations ν. A corresponding procedure starting with a state

$$\hat{c}^\dagger_{\alpha,\sigma}|N_e\rangle_0 , \tag{71}$$

can be used to determine the spectral function for the particle states.

III. RESULTS AND DISCUSSION

First, we checked the LMSPHF–approach discussed in sec. II B for half–filled lattices associated to $N = 2$, $N = 4$ and $N = 6$ sites, respectively. Simple counting of the number of variational variables (see tab. I) shows that for these lattices the approach is exact. Each state can be represented by a single spin– and linear momentum–projected HF–configuration for any value of U/t. This has been tested explicitely for the 36 different states of the half–filled $N = 4$ lattice as well as for the 5 lowest states of each possible linear momentum quantum number with spins $S = 0$, $S = 1$ and $S = 2$ in the half–filled $N = 6$ grid. As an illustrative example we present in Fig. 1 the energy spectrum for the half-filled $N = 4$ lattice as obtained for $U/t = 4$. Each of these states can be represented by a single projected LMSPHF–determinant. The figure also shows nicely the degeneracy of the states with $\xi = 1$ and $\xi = 3$ (or -1) discussed in sec. II A. As expected, the ground states have all total spin $S = 0$, however, while for the lattices with $N = 2$ and $N = 6$ the linear momentum quantum number $\xi = 0$ is obtained, the $N = 4$ ground state has $\xi = N/2 = 2$.

N	4	6	12	14	30
Hilbert restricted space	~ 10	~ 70	$\sim 2\times 10^4$	$\sim 2\times 10^5$	$\sim 10^{14}$
variationnal parameters	32	72	288	392	1800

TABLE I: Comparison of the dimension of the Hilbert restricted space (taking account of the symmetries) for a given half-filled lattice with N sites with the number of parameters involved in the LMSPHF-approach.

This feature persists, if half–filled lattices with larger N are considered : For $N/2$ being an odd integer the ground state has $S = 0$ and $\xi = 0$, while for $N/2$ being an even integer $S = 0$ and $\xi = N/2$ is obtained.
This effect can be understood by a simple spin–correlation. Assume for the moment small interaction strength U. Then, if $N/2$ is odd, the configuration with the lowest energy is obviously the determinant in which the single particle states (3) with $\alpha = 0, \ldots, \pm(N-2)/4$ are all filled, each by two electrons with opposite spin–directions. The resulting total spin is then $S = 0$ and the linear momentum quantum number $\xi = 0$. For $N/2$ being even, however, the situation is different. Here, the last two electrons have to be distributed over the two degenerate states with $\alpha = \pm N/4$.
It can be shown that for two electrons with opposite spin directions occupying two different basis orbits (3) always the $S = 1$ component is energetically favored with respect to the $S = 0$ component. The spin–correlation explains why half–filled lattices with $N/2$ being odd has the lowest excited state associated with total spin $S = 1$ and linear momentum quantum number $\xi = N/2$. Assuming again small interaction strength U, the energetically lowest configurations are obtained by promoting one of the four electrons from the last occupied orbits ($\alpha = \pm(N-2)/4$) to the first unoccupied orbits ($\alpha = \pm(N+2)/4$) in the above mentioned ($S = 0$, $\xi = 0$)–ground state configuration for odd $N/2$. There are 8 degenerate determinants of this type, 4 of them with $\xi = N/2$, 2 with $\xi = 1$ and 2 with $\xi = -1$ (or, equivalent $\xi = N-1$). The expectation value of the Hamiltonian for each of these determinants will be denoted by b. The $\xi = \pm 1$ configurations yield two degenerate $S = 1$ states at energy $b - U/N$ and two degenerate $S = 0$ states at energy $b + U/N$. The four $\xi = N/2$ determinants, however, can be coupled to two $S = 1$ configurations both with energy $b - U/N$ and an interaction of $-U/N$ between them and to two $S = 0$ configurations both with energy $b + U/N$ and an interaction of U/N in between. Thus we get here one $S = 1$ solution with energy $b - 2U/N$, an $S = 1$ and an $S = 0$ solution both having energy b, and one $S = 0$ state with energy $b + 2U/N$. Consequently, here the lowest ($S = 1$, $\xi = N/2$)–solution will become the first excited state. Again the relative splitting in between the various states will even increase with increasing interaction. Also this expectation is confirmed by the results obtained for the half–filled $N = 6$–, $N = 14$– and $N = 30$–lattices in the present work.

A. Half-filled N=12 lattice

Let us now consider the half–filled $N = 12$ lattice. Here in the usual Lanczos approach (all $\Sigma = 0$ determinants) already 853 776 configurations have to be treated, and even using all the symmetries, for $S = 0$ and the 12 possible ξ–values still between 18 840 and 18 916, for $S = 1$ and the possible ξ–values between 31 833 and 31 872 configurations have to be accounted for. Fig. 2 displays the energies of the first excited states for various methods using an interaction strength of $U/t = 4$. In the rightmost column (EXACT) the results of the Lanczos diagonalisation for the lowest 4 states are presented, the other columns refer to different variational approaches. The leftmost one (HF) gives the Hartree-Fock result obtained by using the determinant (12) as test wave function and not caring about spin– and linear momentum. The next two columns have been obtained by HF calculations with linear momentum projection before the variation only (LMPHF) but still not restoring the total spin and with spin–projection before the variation only (SPHF) but not restoring the total linear momentum. The next column (LMS$_z$PH) results from variational calculations with projection on good linear momentum and z–projection of the spin $S_z = 0$. Finally, the second but last column (LMSPHF) presents the results obtained for the lowest 5 states with linear momentum– and full spin–projection before the variation as described in sec. II B. As can be seen, the LMSPHF–approach reproduces the energies of the exact solutions not only for the ground but also for the lowest excited states very well. The deviations vary only between 0.16 and 0.58 percent. This is remarkable since the number of variational parameters (288 for $S = 0$ in this case) is significantly smaller than the dimension of the space with good symmetries, which is 18840 in this example.
As expected from the above arguments based on spin–correlation the ground state has $S = 0$ and $\xi = N/2 = 6$, while for the quantum numbers of the first excited state $S = 1$ and $\xi = 0$ are obtained. It is furthermore obvious, that both, linear momentum and spin have to be restored simultaneously. All results obtained by performing none or only part of the corresponding projections fail to reproduce the exact spectrum.
Fig. 3 presents the energies of lowest $S = 0$, $S = 1$ and $S = 2$ states obtained with the LMSPHF–approach for the various linear momentum quantum numbers ξ. Note, that the $\xi = 1$–results are degenerate with those for $\xi = 11$,

those for $\xi = 2$ with those for $\xi = 10$, etc., so that only the results for $\xi = 0, \ldots 6$ are shown. Except for the $(S = 0, \xi = N/2)$–ground state, the lowest states for all other linear momentum quantum numbers have total spin $S = 1$. This supports again the importance of the above discussed spin–correlation.
In fig. 4, we represent the occupation numbers of the various basis orbitals (3) in the LMSPHF–ground state obtained via eq. (67) and we compare it with those resulting from the one–body density of the exact ground state and with those expected for a non–interacting Fermi–gas. Again, excellent agreement of the LMSPHF–results with the exact solution is obtained. It should be stressed, that the occupation numbers obtained via eq. (67) are not affected by the number of determinants m used for the calculation of the hole–spectral functions. Identical numbers are obtained, no matter whether only the ground state determinant $|D^1\rangle$ $(m = 1)$ or, e.g., all the $m = 5$ determinants corresponding to the five lowest LMSPHF–solutions Fig. 2 are included in the calculation.
In fig. 5, we compare the occupation numbers of the basis orbitals in the LMSPHF–$(S = 0, \xi = 6)$–ground states obtained for various strength parameters U/t of the interaction. Since in all cases the LMSPHF– and exact occupation numbers cannot be distinguished, we have plotted only the former. As expected, the correlations (i.e, the deviation from the Fermi–gas values) grow with increasing interaction. Already at $U/t = 64$ the result looks rather similar to the equal distribution of the anti-ferromagnetic limit expected for $U/t \to \infty$.
In fig. 6 we represent the hole– (eq. (65)) and particle– (eq. (66)) spectral functions versus the excitation energy ω (in units of t). Here, $\omega = \epsilon_{\tilde{h}}$ for the hole– and $\omega = \epsilon_{\tilde{p}}$ for the particle–states, respectively. We compared the results obtained by using only one determinant $(m = 1$, upper half of the figure) with those resulting from using the HF–transformations obtained for all the $m = 5$ lowest LMSPHF–states presented in Fig. 2. As expected for the half–filled lattice, particle– and hole–states are nicely symmetric around the Fermi–energy $\omega_F = U/t/2$. They are separated by the so–called "Hubbard–gap" of about $U/t/2$. Using $m = 5$ determinants one obtains 120 hole and 120 particle states for each possible linear momentum quantum number, while we obtain only 24 states for $m = 1$ for each $\xi_{\pm 1}$–value. Consequently, the strength is more spread for the $m = 5$–approximation with respect to the more restricted $m = 1$–approximation.
Finally, in Fig. 7 we compare the results for the strength defined by eq. (66) and obtained with $m = 5$ determinants for $S = 1/2$ and $\xi = 0, \ldots, 3$ with those resulting from the exact calculation as described in (69) - (71). As can be seen, the agreement for both the excitation energies as well as for the splitting of the strength is again very good.

B. Doped lattice

Let us now consider a system of only 10 electrons in the $N = 12$–lattice, again using $U/t = 4$ as interaction strength. $N_e/2$ is odd, then all the basis orbits (3) with $\alpha = 0, \pm 1$ and ± 2 can be filled, each with two electrons with opposite spin directions. Thus, from spin–correlation argument, one expects an $(S = 0, \xi = 0)$–ground state. The lowest excited states can then be obtained by promoting one of the four electrons from the $\alpha = \pm 2$–orbitals to the $\alpha = \pm 3$ orbits. There are again 8 degenerate determinants of this type : 2 with $\xi = 1$, 2 with $\xi = -1$, 2 with $\xi = 5$ and 2 with $\xi = -5$. Calling $\mathcal{C}$ the expectation value of the Hamiltonian (5) within each of these determinants, one obtains four degenerate $S = 1$ states at energy $\mathcal{C} - U/N$ and four degenerate $S = 0$ states at energy $\mathcal{C} + U/N$, respectively. The corresponding linear momentum quantum numbers are in both cases $\xi = 1, -1, 5$ and -5. Thus one expects the lowest excited states to have $S = 1$ and $\xi = \pm 1, \pm 5$.
Fig. 8 presents the energies of lowest $S = 0$, $S = 1$ and $S = 2$ states of the 10–electron system on the $N = 12$–lattice obtained with the LMSPHF–approach for the various linear momentum quantum numbers $\xi = 0, \ldots 6$. As in Fig. 3, the spectra for $\xi = -1, \ldots, -5$, which are degenerate with those for $\xi = 1, \ldots 5$ have not been plotted. As expected, we obtain an $(S = 0, \xi = 0)$–ground state, and the lowest four excited states have all $S = 1$ and linear momentum quantum numbers of $\xi = \pm 1$ and $\xi = \pm 5$, respectively.
Obviously, the nice particle–hole symmetry in the spectral functions of the half–filled $N = 12$–lattice is destroyed, if only 10 electrons in this lattice are considered. Using the simplest $(m = 1)$ approximation for the calculation of the $S = 1/2$–wave functions for the 9– and 11–electron systems, one obtains here for each possible linear momentum 20 one–hole– and 28 one–particle–states. This is reflected in the hole– and particle–spectral functions, which are shown in Fig. 9 as a function of the excitation energy. Particle– and hole–strengths are now distributed asymmetrically around the Fermi–energy and furthermore, the Hubbard–gap obtained for the half–filled lattice has vanished.

C. N=14 lattice

We shall now consider the half–filled $N = 14$–lattice, again using $U/t = 4$. Here, in the usual Lanczos–approach (all determinants with $\Sigma = 0$) already 11 778 624 determinants have to be treated. Consequently, for this example we could obtain only the exact ground and first exited state within about one week of computer time. Even if all the

symmetries would be used, for $S = 0$ and the 14 possible linear momentum quantum numbers still between 197 099 and 197 276, for $S = 1$ and the possible ξ–values between 357 770 and 357 945 configurations have to be accounted for.
In fig. 10, we display the results for the lowest states obtained with different variational methods and compare them with the exact results. The nomenclature is the same as in Fig. 2. Again it is seen, that all results obtained by performing none or only part of the symmetry–projections fail to reproduce the exact spectrum. Only if linear–momentum and full spin–projection are both performed simultaneously before the variation as done in the LMSPHF–approach the exact data can be reproduced. The deviation of the LMSPHF–energies from the latter amount here to 0.38 percent for the ground and 0.93 percent for the first excited state, respectively. Thus (as expected because of the considerably larger dimensions) they are larger than in the half–filled $N = 12$–example. It should be stressed, however, that in the LMSPHF–approach each of these states are represented by only a single symmetry–projected configuration. Correlating these solutions by additional determinants could, obviously, still improve the agreement. As expected for a half–filled lattice with $N/2$ being odd, the ground state has total spin $S = 0$ and linear momentum quantum number $\xi = 0$, while for the first excited state $S = 1$ and $\xi = N/2 = 7$ is obtained.
In fig. 11 we represent the energies of the lowest $S = 0$, $S = 1$ and $S = 2$ states obtained with the LMSPHF–approach for the various linear momentum quantum numbers ξ. Again, the spectra for $\xi = N/2+1, \ldots, (N-1)$ are degenerate with those obtained for $\xi = 1, \ldots N/2-1$, respectively, and are hence not displayed. Except for the $(S = 0, \xi = 0)$–ground states and the $\xi = 2$ case, where the lowest $S = 0$ and $S = 1$ states are almost degenerate, the lowest states for all the other linear momentum quantum numbers have always total spin $S = 1$. This supports the above discussed spin–correlation favoring the $S = 1$–excitations.
Also for the half–filled $N = 14$–lattice, the LMSPHF– and exact occupation numbers of the ground state can hardly be distinguished and are not shown here. Instead, we present in Fig. 12, the hole– and particle–spectral functions obtained with the $m = 5$ HF–transformations resulting from the five lowest LMSPHF–solutions out of Fig. 10. In order to obtain continuous functions of the excitation energy $\omega = \epsilon_{\tilde{h}}$ (or $\omega = \epsilon_{\tilde{p}}$), each state has been broadened with a Lorentzian of constant width 0.05 t. As can be seen, the particle– and hole–strengths are symmetrically distributed around the Fermi–energy (again $\omega_F = U/t/2$) and separated by a Hubbard–gap of about the same size ($U/t/2$) as obtained for the half–filled $N = 12$–lattice.

D. Large N=30 lattice

Finally, we shall report LMSPHF–results for the half–filled $N = 30$–lattice, again for interaction strength $U/t = 4$. Here in the usual Lanczos–approach $2.9 \cdot 10^{15}$ states would have to be included, which is obviously impossible. Even coupling the configurations to good total spin and linear momentum quantum number, still for the various ξ–values dimensions of the order of $9.7 \cdot 10^{13}$ for $S = 0$ and even $2.2 \cdot 10^{14}$ for $S = 1$ would have to be treated. In the LMSPHF–approach, however, for each $S = 0$–state "only" functions of 1800 real variables have to be minimized.
As in Figs. 2 and 10 we present the results for the energies of the lowest states as obtained with various variational methods for the half–filled $N = 30$–lattice in Fig. 13. Obviously, there is no exact result available to compare with. According to the spin coupling arguments, since $N/2$ is odd the ground state has $S = 0$ and linear momentum quantum number $\xi = 0$ while the first excited state is obtained for $S = 1$ and $\xi = N/2 = 15$. Again it is seen that the simultaneous restoration of linear momentum and total spin before the variation as done in the LMSPHF–approach is essential. All other approximations produce results, which do not come close to the LMSPHF–energies.
The occupation numbers for the different basis states (3) in the LMSPHF–ground state are presented in comparison with the values expected for a non–interacting Fermi–gas in Fig. 14. Like for the half–filled $N = 12$ lattice (see Fig. 4), strong effects of the correlations are observed.
The density of states $N(\omega)$ (eq. (68)) for the half–filled $N = 30$–lattice is shown in Fig. 15. Here, we have performed a simple 1–determinant calculation ($m = 1$) as explained in sec. II C. Again, the states were broadened by a Lorentzian with a width of 0.05 t. As expected for half–filling, particle– and hole– strengths are distributed symmetrically. The Fermi–energy is again $\omega_F = U/t/2$ and the width of the Hubbard–gap again of about the same size as obtained for the half–filled $N = 12$– and $N = 14$–lattices (see figs. 6 and 12). .
Finally, in Fig. 16, the particle– and hole–spectral functions are presented as functions of linear momentum k and excitation energy ω. Again, Lorentz–shape and a constant width of 0.05 t has been used. Obviously, the strength of each of these spectral functions would still be redistributed, if instead of only one, several determinants would be taken into account for the calculation. Since anyhow, there are no "exact" (or experimental) data to compare with, this generalization has not been done for the $N = 30$–lattice in the present investigation.

IV. CONCLUSIONS

We have devised a variational approach for the approximate solution of the 1–dimensional Hubbard–model with nearest neighbor hopping and periodic boundary conditions. For the ground state we start with a Hartree–Fock type transformation mixing all the quantum numbers of the single electron basis states.
The results may be summarized as follows :
For many–electron systems on small lattices, where the number of configurations to be treated for each pair of good spin– and linear momentum–quantum number is smaller than the number of real variational degrees of freedom accounted for in the variational calculation, the LMSPHF–approach is obviously exact. However, even in the half–filled $N = 12$– and $N = 14$–lattices, where for each pair of quantum numbers (S, ξ) the number of configurations is by 2 or even 3 orders of magnitude larger than the number of variational degrees of freedom, the LMSPHF–approach does reproduce the exact energies of the ground and lowest excited states with an accuracy of better than 99 percent, the occupation numbers of the ground and lowest excited states even better, and yields (at least if several determinants for the calculation of the one–hole and one–particle spectra are included) even for the spectral functions very good agreement with the exact results. This gives some confidence, that the LMSPHF–approach can be considered as a very good truncation scheme even for lattices which are far too large to allow for exact diagonalisation. Even where complete diagonalisation via the Lanczos method is still numerically possible, the LMSPHF–approach is much faster.
Spin– and linear momentum– quantum numbers for the ground and the lowest excited state can reliably be predicted making use of the fact that for two electrons with opposite spin–directions in two different momentum space basis orbits always the $S = 1$–configuration is energetically favored with respect to the $S = 0$–one. Thus, for half–filled lattices with $N/2$ being odd the ground state has $S = 0$ and linear momentum $\xi = 0$, while the lowest excited state has $S = 1$ and $\xi = N/2$. For half–filled lattices with $N/2$ even on the other hand one obtains $S = 0$ and $\xi = N/2$ for the ground and $S = 1$ and $\xi = 0$ for the first excited state. The same spin–correlation can be used to predict the quantum numbers of the lowest states away from half–filling and is also supported by the observation that for almost all linear momentum quantum numbers (except for that of the ground state) the lowest state has always total spin $S = 1$.
One of the nicest features of the LMSPHF–method is that it still can be improved rather easily. So, e.g., instead of HF–determinants generalized Slater–determinants of the HF–Bogoliubov (HFB) type can be used as basic building blocks. This would increase the number of real variational degrees of freedom (for the example of an $S = 0$–state) from $2N_e(2N - 2N_e)$ in the LMSPHF–approximation to $2N(2N - 1)$ for any number of electrons. The price one has to pay for this, is an additional integration due to the (then necessary) projection onto good total electron number in the calculation of all the matrix–elements. Because of the simple form of the interaction, however, this should not cause any serious problems. The resulting linear momentum–, spin– and number projected HFB–approach would consequently account for considerably more correlations in each single configuration than the LMSPHF–method.
Furthermore, instead of using essentially only one symmetry–projected configuration for each state, correlating symmetry–projected configurations can be added and the underlying HF– (or HFB–) transformations again be determined by variational calculations. Since the energy gain obtained for a particular state under consideration due to the last added configuration is by construction always smaller than the energy gain due to the last configuration added before, this procedure (which already has been applied successfully to the nuclear many–body problem [3]) can also give a hint on the quality of the solution even in lattices, which are too large to allow for an exact solution.
Last but not least, the procedure discussed in the present work can be extended easily to the 2–dimensional Hubbard–model, which is supposed to be of larger physical relevance than its 1–dimensional simplification. Then, obviously, the total linear momentum becomes a 2–dimensional vector and one has to project on each of its components separately. Thus again, with respect to the LMSPHF–approach discussed above only one additional integration is needed.
This leaves ample space for future investigations and we are quite confident that the variational approaches originally devised for the nuclear many–body problem will turn out to be rather useful even for more complicated lattice Fermion models than the simple 1–dimensional version investigated in the present work.

Acknowledgments

We are grateful that the present study has been supported by a grant from the Ministry of Science, Research and the Arts of the state Baden–Württemberg (Az : 24-7532.23-19-18/1 and /2) to JM via the Landesforschungsschwerpunkt

"Quasiteilchen".

---

[1] B.A.Brown, Prog.Part.Nucl.Phys. **47**, 517 (2001).
[2] F. Gebhard, "The Mott Metal–Insulator Transition", Springer tracts in modern physics, Vol. 137, 1997.
[3] K.W.Schmid, Prog.Part.Nucl.Phys. **52**, 565 (2004).
[4] P. Fulde, "Electron Correlations in Molecules and Solids", Springer Series in Solid–State Sciences, Vol. 100, 3rd edition, 1995, chapter 2.
[5] see for example K. J. Szczepanski, P. Horsch, W. Stephan, and M. Ziegler, Phys. Rev. B **41**, 2017 (1990) and references therein.
[6] see for example S. R. White, D. J. Scalapino, R. L. Sugar, E. Y. Loh, J. E. Gubernatis, and R. T. Scalettar, Phys. Rev. B **40**, 506 (1989).
[7] S. C. Pieper and R. B. Wiringa, Ann. Rev. Nucl. Part. Sci. **51**, 53 (2001).
[8] T.Otsuka, M.Homma, T.Mizusaki, N.Shimizu, Y.Utsumo, Prog.Part.Nucl.Phys. **47**, 319 (2001).
[9] F.Villars in: C. Bloch(ed.) Varenna Lectures, Academic Press, New York 1966, p.1 .
[10] P. Ring, P. Schuck, *The Nuclear Many–body Problem* (Springer, Berlin–Heidelberg–New York, 1980).
[11] D.J. Thouless, Nucl.Phys. **21**, 225 (1960).
[12] K. W. Brodlie in "The State of the Art in Numerical Analysis", ed. D. Jacobs, Academic Press (N.Y.) 1977, p. 228.
[13] W.H. Press, B.P. Flannery, S.A. Teukolsky, and W.T. Vetterling, "Numerical Recipes", Cambridge University Press,, 1992, p. 418.
[14] H. Müther and L.D. Skouras, Phys. Lett. **B 306**, 201 (1993).

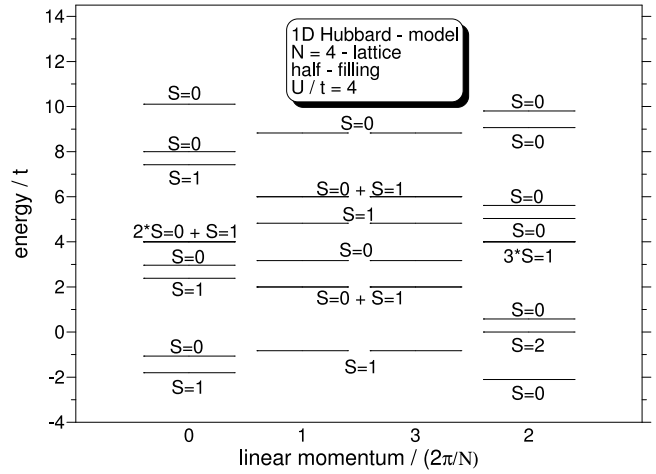

FIG. 1: Energy spectrum of the half–filled $N = 4$–lattice as obtained with interaction strength $U/t = 4$ either by complete diagonalization or by the LMSPHF–approach out of sec. II B. In the latter case each of the states is represented by a single linear momentum– and spin–projected Slater–determinant.

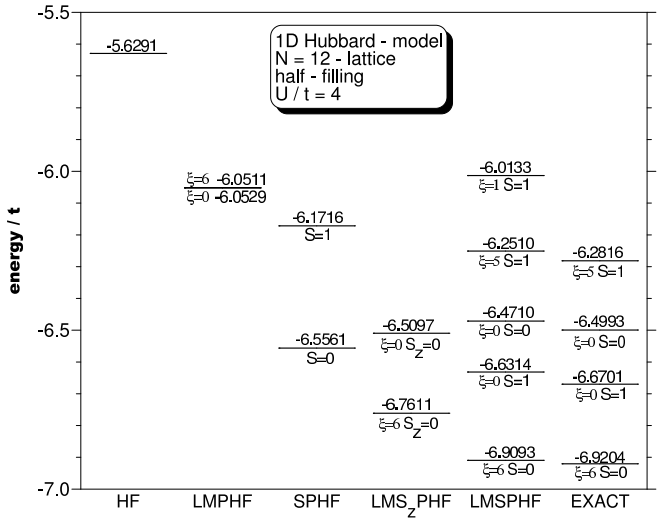

FIG. 2: Energies for some states of the half–filled $N = 12$–lattice as obtained using the interaction strength $U/t = 4$ by various approaches. The different columns refer to a simple unprojected HF–calculation (HF), to HF with only linear momentum– (LMPHF), or only spin–projection (SPHF) before the variation and to HF with restoration of the total linear momentum and only the 3–component of the total spin (LMS_zPHF). Finally, the energies of the lowest few states obtained with linear momentum– and full spin–projection before the variation as described in sec.II B (LMSPHF) are compared with those resulting from a complete diagonalization (EXACT).

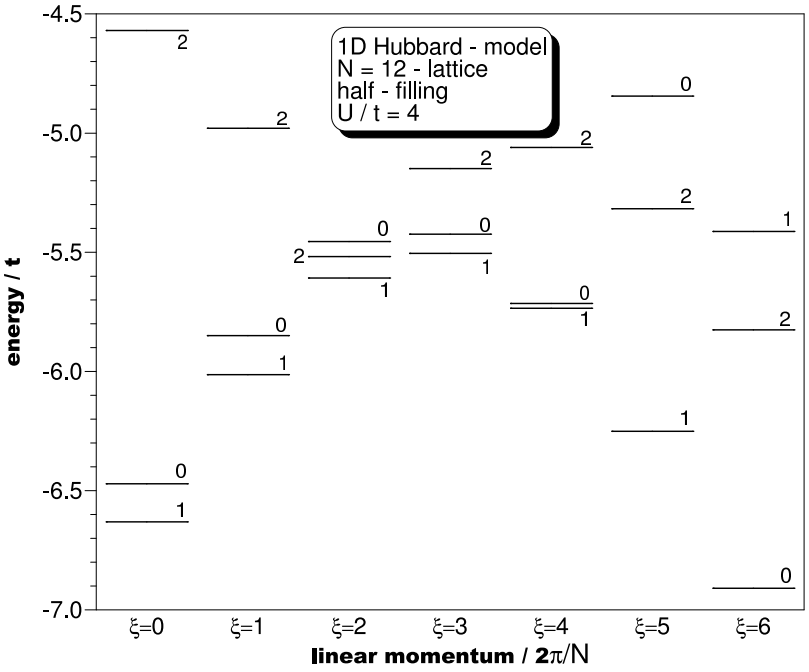

FIG. 3: Again for the half–filled $N = 12$–lattice and $U/t = 4$, the energy spectra for the lowest $S = 0$, $S = 1$ and $S = 2$ states as obtained with the LMSPHF–method for the various linear momentum quantum numbers ξ are displayed. Because of the degeneracy of the $\xi = 12 - i$ with the $\xi = i$ spectra for $i = 1, \ldots, 5$, only the spectra for $\xi = 0, \ldots 6$ are presented.

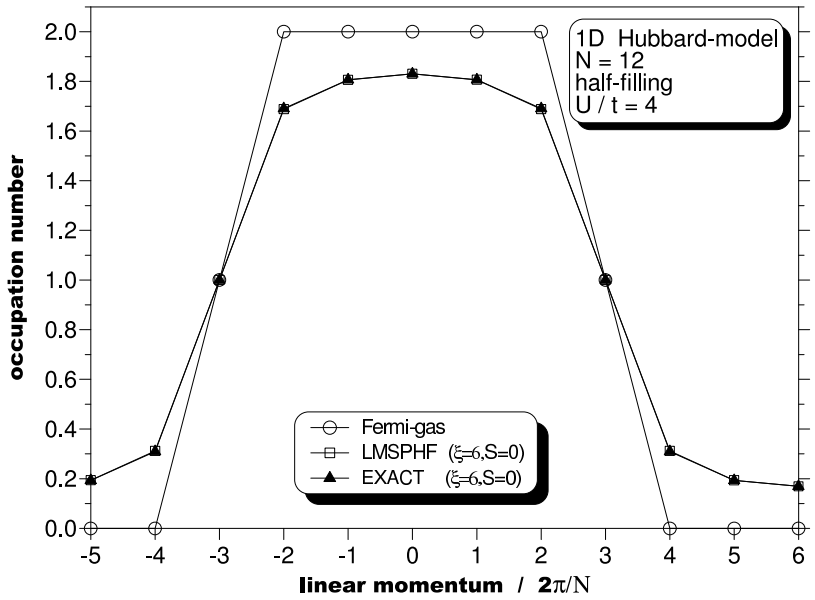

FIG. 4: For the half–filled $N = 12$–lattice and $U/t = 4$ the occupation numbers (eq. (66)) of the various basis states in the $(S = 0, \xi = 6)$–LMSPHF–ground state are compared to those obtained by a complete diagonalization (EXACT) and to those expected for a non–interacting Fermi–gas. Identical occupation numbers are obtained for using only the lowest $(m = 1)$ or the lowest five $(m = 5)$ determinants in the calculation of the hole–spectral functions.

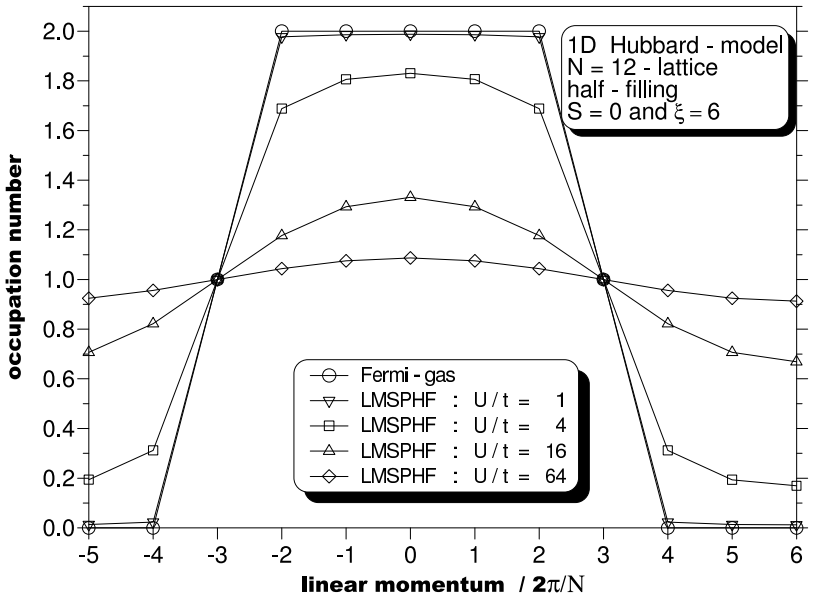

FIG. 5: Same as in Fig. 4, but for various interaction strengths U/t. Since in all cases the exact and LMSPHF-results cannot be distinguished, only the latter are displayed.

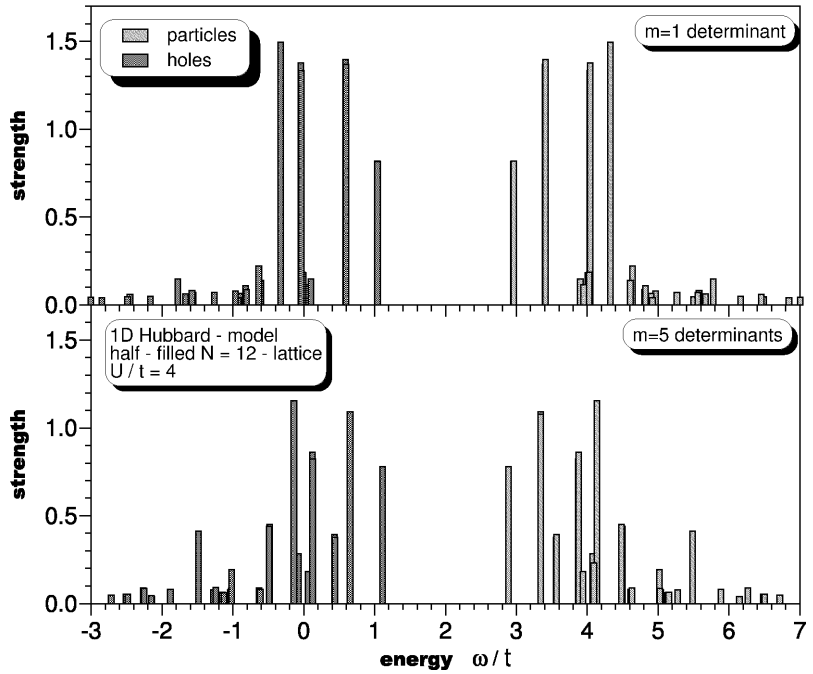

FIG. 6: Again for the half–filled $N = 12$–lattice and $U/t = 4$, the hole– (eq. (65)) and particle– (eq. (66)) spectral functions are plotted for all possible values of $\xi_{\pm 1}$ as functions of the energy ω ($= \epsilon_{\tilde{h}}$ and $= \epsilon_{\tilde{p}}$, respectively). The upper part of the figure has been obtained by using only the ground state determinant $|D^1\rangle$ in the calculation for the spectral functions ($m = 1$). Using instead all the $m = 5$ determinants corresponding to the lowest five states out of Fig. 2 in these calculations, one obtains the results displayed in the lower part of the figure.

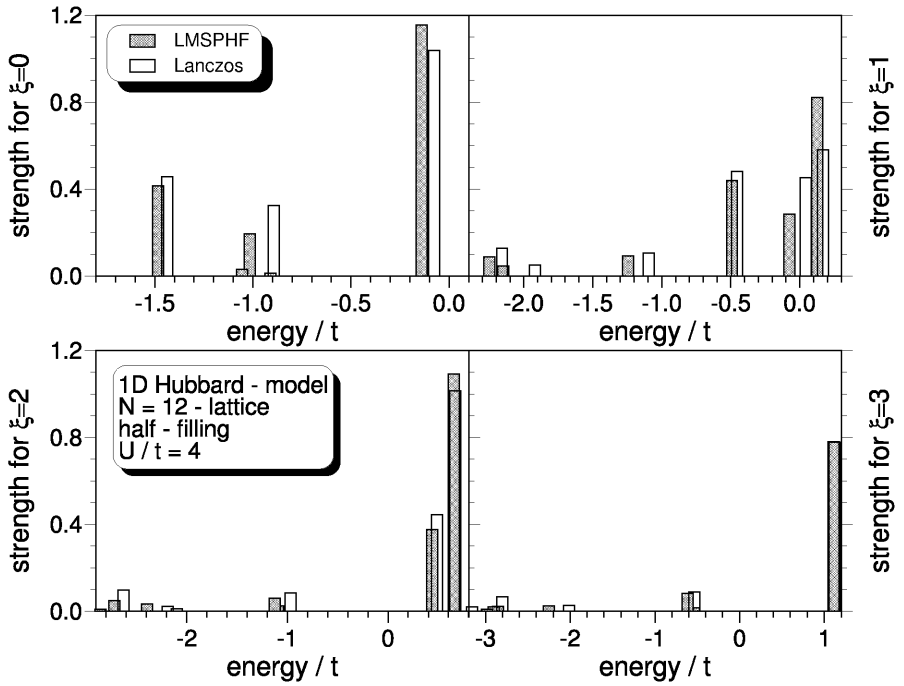

FIG. 7: Again for the half–filled $N = 12$–lattice and $U/t = 4$, the hole spectral functions for $\xi = 0, \ldots, 3$ as obtained with $m = 5$ determinants are plotted versus the excitation energy and compared with the "exact" results computed with the Lanczos–approach as discussed in the text.

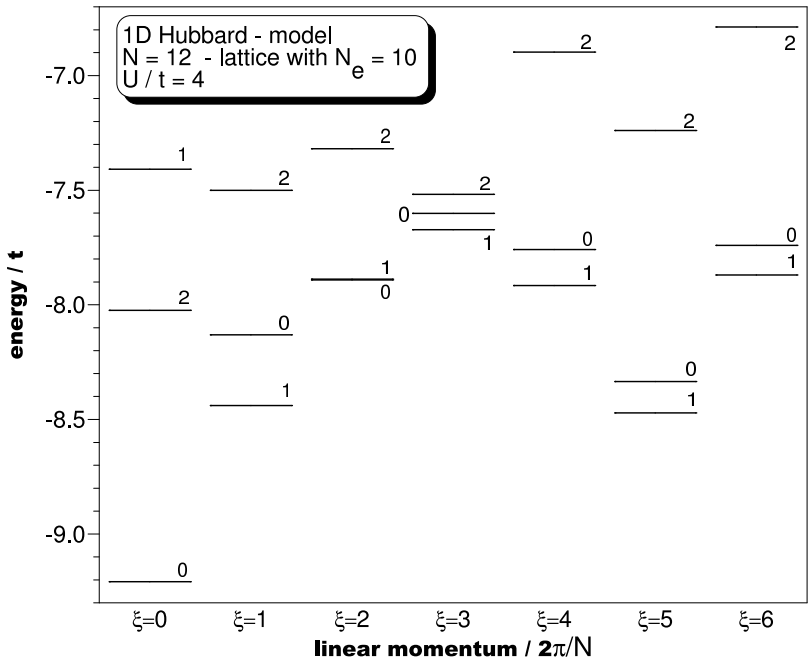

FIG. 8: Same as in Fig. 3, but for only 10 electrons in the $N = 12$–lattice.

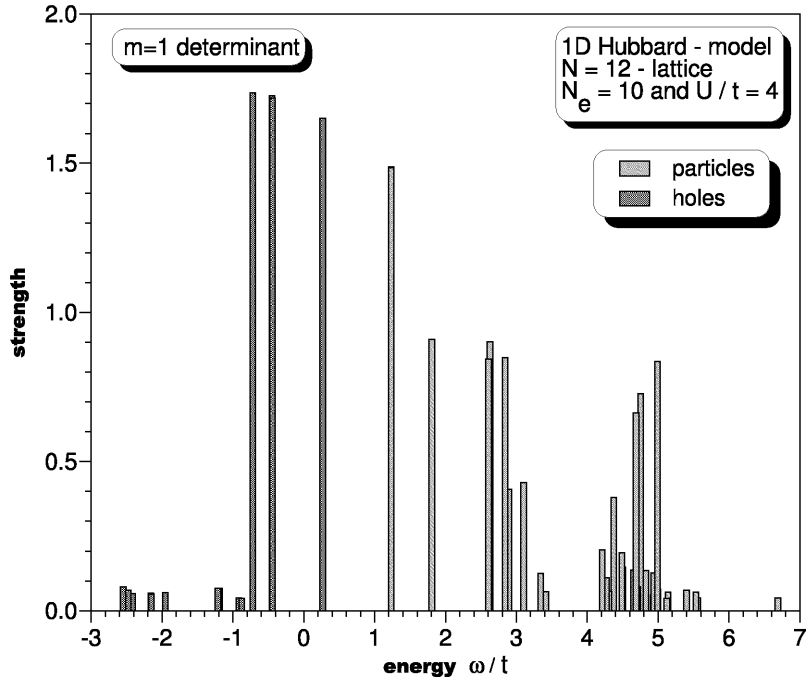

FIG. 9: Same as in Fig. 6, but for only 10 electrons in the $N = 12$–lattice. Here only the results obtained with one determinant ($m = 1$) are presented.

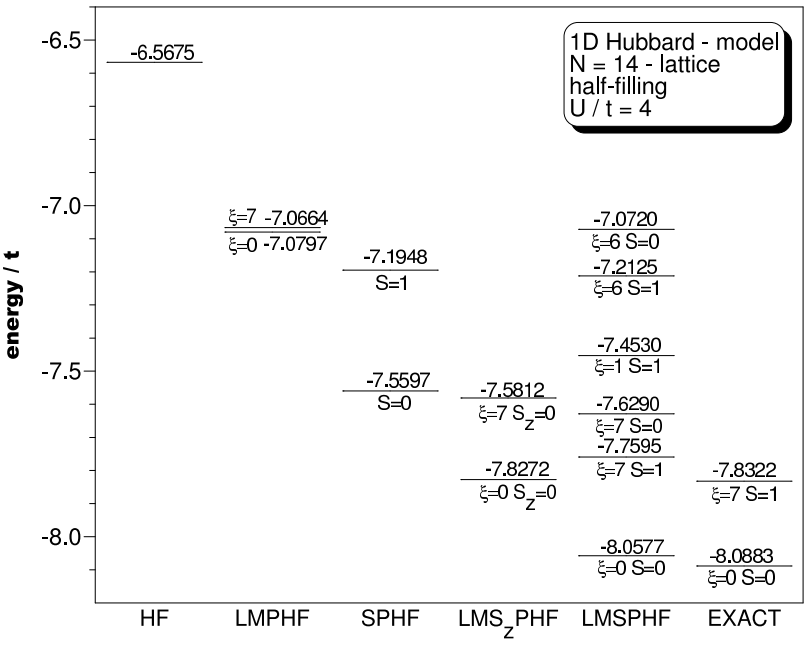

FIG. 10: Same as in Fig. 2, but for the half–filled $N = 14$–lattice.

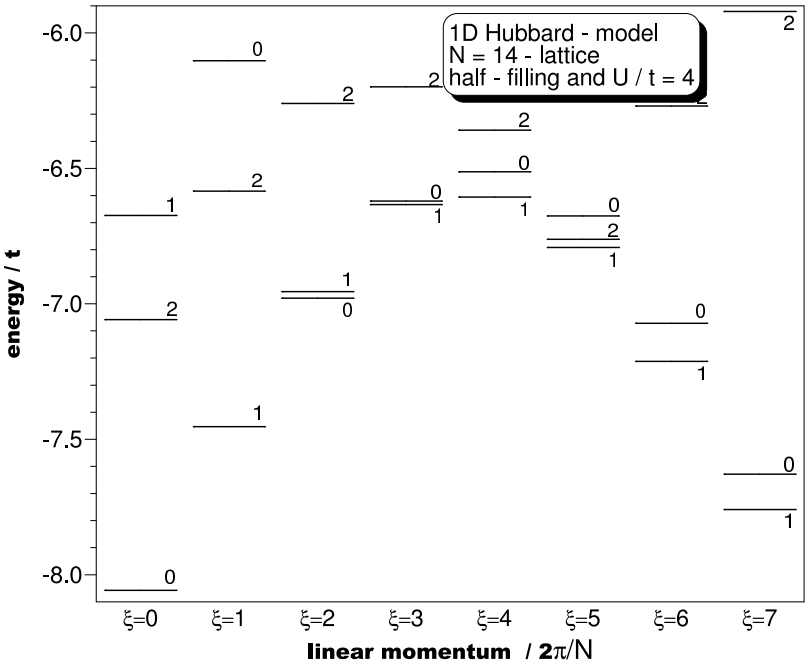

FIG. 11: Same as in Fig. 3, but for the half–filled $N = 14$–lattice.

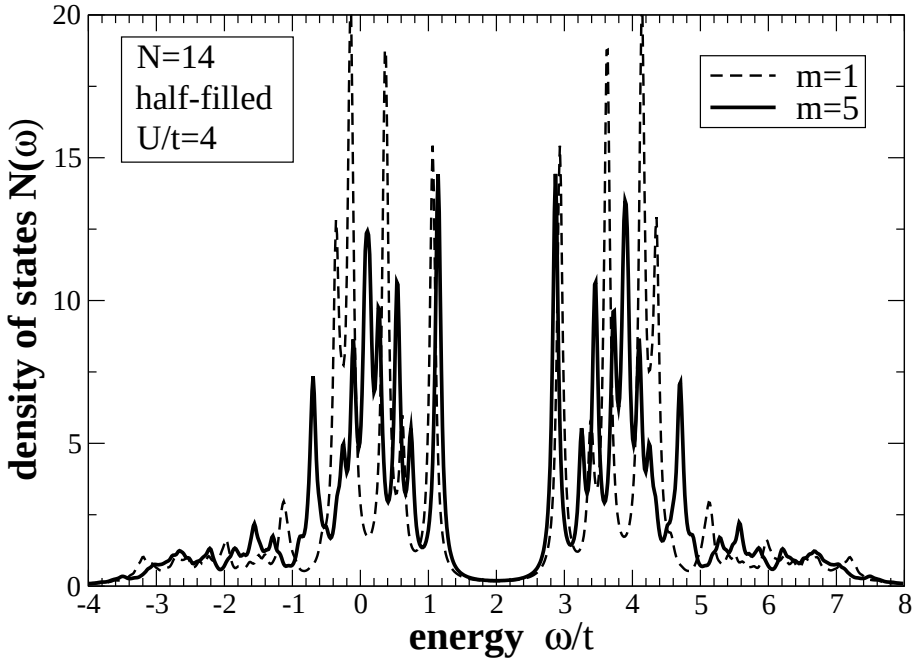

FIG. 12: Again for the half–filled $N = 14$–lattice, the sum of the hole– and the particle–spectral function are displayed as functions of the excitation energy ω (in units of t) and the linear momentum k in units of $(2\pi/N)$. The spectral functions have been obtained here by using the $m = 5$ determinants corresponding to the five lowest LMSPHF–solutions in Fig. 10. In order to obtain continuous functions for each state a Lorentz–shape with constant width of 0.05 t has been used.

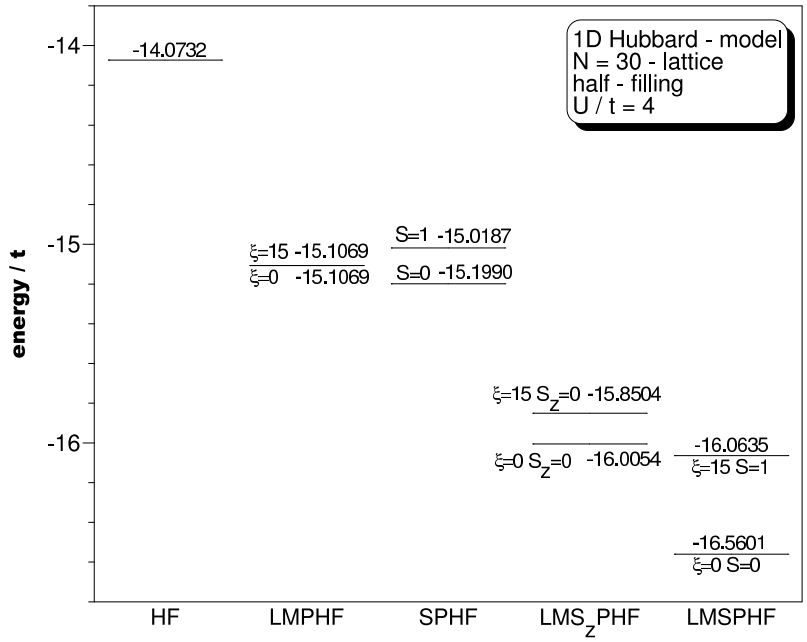

FIG. 13: Same as in Fig. 2, but for the half–filled $N = 30$–lattice. Again $U/t = 4$. Here no exact results are available to compare with.

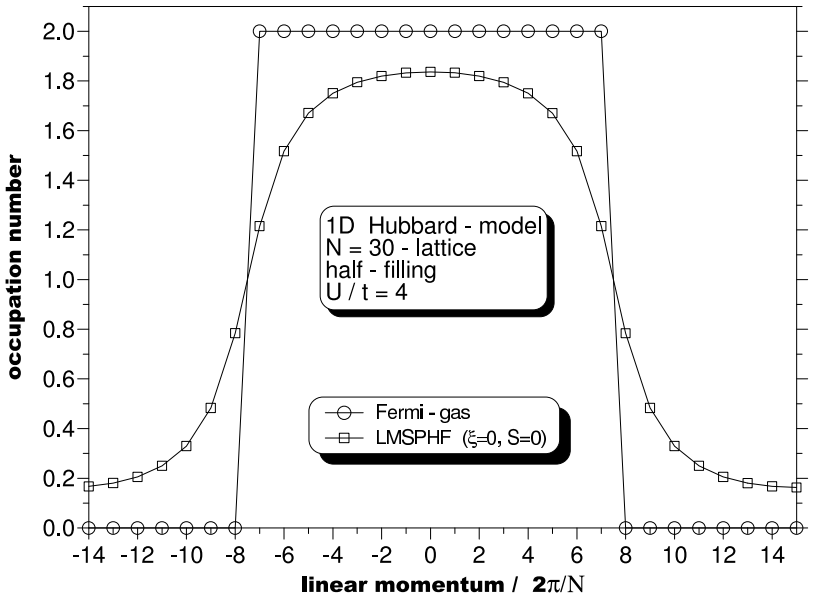

FIG. 14: Same as in Fig. 4, but for the half–filled $N = 30$–lattice. Again $U/t = 4$, and no exact results are available.

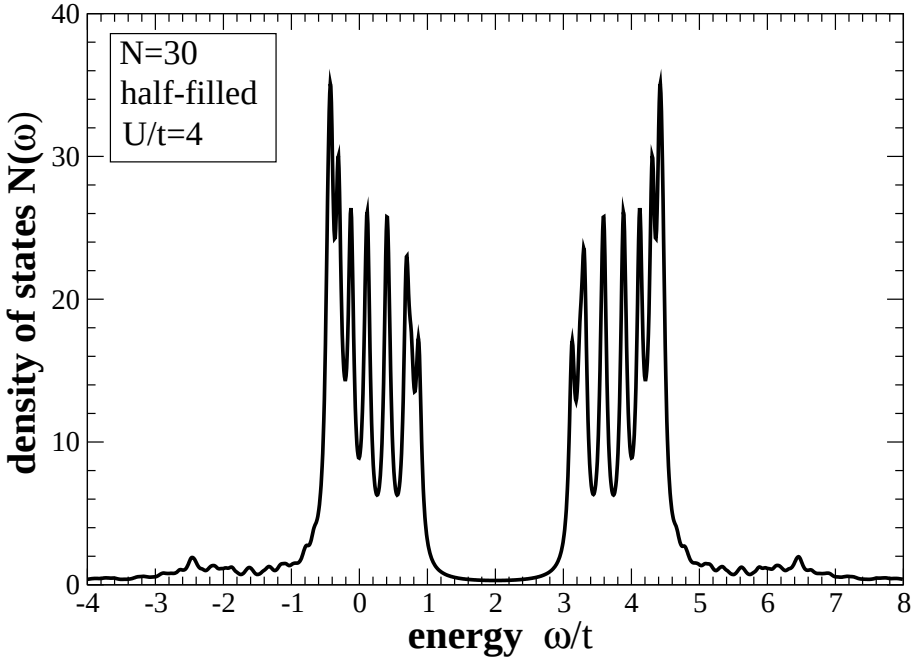

FIG. 15: For the half–filled $N = 30$–lattice with $U/t = 4$ the total number of states $N(\omega)$ out of eq. (68) is presented as function of the excitation energy. Here only $m = 1$ determinant was used to obtain the one–hole– and one–particle states. Each of these states has been artificially broadened to a Lorentz–shape with constant width of 0.05 t.

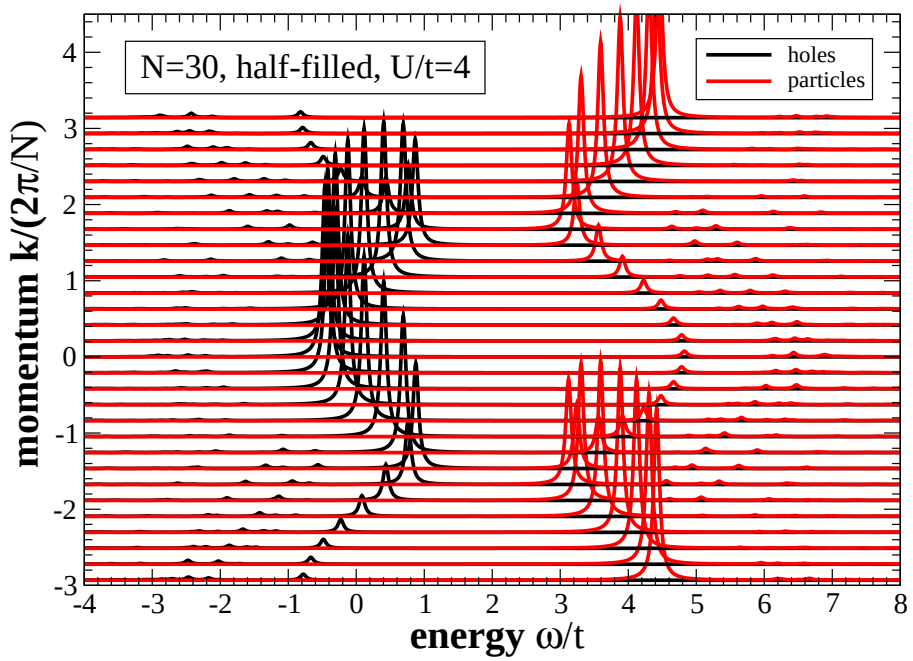

FIG. 16: (Color online) Same as in Fig. 12, but for the half–filled $N = 30$–lattice, and using only $m = 1$ determinant in the calculation of the spectral functions.